INITIAL STATE ESTIMATION FOR A GUN LAUNCHED PROJECTILE IN A SPATIALLY VARYING MAGNETIC FIELD

by
Feni Chawla

A THESIS

submitted to

Oregon State University

in partial fulfillment of
the requirements for the
degree of

Master of Science

Presented June 13, 2006
Commencement June 2007

AN ABSTRACT OF THE THESIS OF

Feni Chawla for the degree of Master of Science in Electrical and Computer Engineering presented on June 13, 2006.

Title: Initial State Estimation for a Gun Launched Projectile in a Spatially Varying Magnetic Field

Abstract approved:

Mark F. Costello Molly H. Shor

Smart weapons promise to provide leap ahead capability with regard to accuracy and engagement range for medium and large caliber projectiles. One of the most critical components of a smart weapon system is its sensor suite that provides position, orientation, and velocity information as the projectile flies down range so that effective control action can be taken in flight. Great strides have been made in creating very small and rugged Inertial Measurement Units (IMU) using MEMS accelerometers and vibrating gyroscopes. However, all IMU systems operate by integrating accelerometer and gyroscope measurements. Thus, they must be initialized at launch to produce sufficiently accurate position and orientation data. Due to inherent uncertainty in shot-to-shot launch conditions, for gun launched projectiles, initial conditions cannot be adequately specified by the firing platform like it can with aircraft and missiles. Currently, there is no adequate method to initialize IMU sensor suites on gun launched munitions.

This thesis investigates a novel concept for determining the full state of a projectile near the muzzle of the gun. The methodology relies on the gun system inducing a known spatially varying magnetic field in the vicinity of the muzzle of the gun. Using readings from a cluster of magnetometers embedded within the projectile, the full state of the projectile is determined by solving a nonlinear set of equations.

Master of Science thesis of Feni Chawla presented on June 13, 2006.

APPROVED:

Co-Major Professor, representing Electrical and Computer Engineering

---

Co-Major Professor, representing Electrical and Computer Engineering

---

Director of the School of Electrical Engineering and Computer Science

---

Dean of the Graduate School

I understand that my thesis will become a part of the permanent collection of Oregon State University libraries. My signature below authorizes release of my thesis to any reader upon request.

Feni Chawla, Author

ACKNOWLEDGEMENTS

I would like to express my sincere gratitude to Dr. Mark Costello for his patience, guidance, encouragement and support during my graduate study. He proved to be an extremely understanding person who extended his full support to my work and at the same time was refreshingly critical of it.

I would like to thank Dr. Molly Shor who considered me worthy enough to work under her guidance, and without whose support it would not have been possible to complete this project.

I would like to extend my gratitude towards Dr. Robert Higdon and Dr. Mei Lien for sparing their valuable time and being on my committee.

I am grateful to the office staff of the Electrical and Computer Engineering, and Mechanical Engineering Departments. My special thanks to my family and friends for their love and support.

TABLE OF CONTENTS

Page

1. INTRODUCTION……1

1.1. OUTLINE 1

1.2. ORGANIZATION OF THE THESIS 2

2. BACKGROUND……3

2.1. SMART WEAPON SYSTEMS 3

2.2. INERTIAL NAVIGATION FOR SMART WEAPONS 3

3. INITIAL STATE ESTIMATION……6

3.1. RIGID BODY MODEL OF PROJECTILE 6

3.2. REFERENCE FRAME RELATIONSHIPS 8

3.3. PROJECTILE STATE VARIABLES 10

3.4. MAGNETOMETER SENSOR READINGS 12

3.5. PROJECTILE INITIAL STATE ESTIMATION 19

3.5.1. Enhanced Newton's Method 19

3.5.2. Non Linear Regression 23

4. IMPLEMENTATION AND RESULTS……..26

4.1. EXPERIMENTAL SETUP AND PROCEDURE 26

4.2. STATE ESTIMATION WITHOUT SENSOR NOISE 28

4.2.1. Bar Magnet Magnetic Field 28

TABLE OF CONTENTS (continued)

Page

4.2.2. Rectangular Loop Magnetic Field 31

4.3. STATE ESTIMATION WITH SENSOR NOISE 33

4.3.1. Bar Magnet Magnetic Field 33

4.3.2. Rectangular Loop Magnetic Field 36

4.4. TRADE STUDIES 40

4.4.1. Variation of Error with Sensor Noise Level 40

4.4.2. Variation of Error with Data Burst Period 42

4.4.3. Variation of Error with Number of Magnetometers 45

5. CONCLUSION 47

5.1. DISCUSSION OF THE RESULTS 47

5.2. SCOPE FOR FUTURE WORK 50

LIST OF FIGURES

Figure Page

3.1: Projectile Geometry with respect to Inertial, Body and Sensor Reference Frames 7

3.2: Euler Angle Geometry of a Projectile with respect to Inertial Frame ... 8

4.1: Selection of a data burst of a nonlinear sequence of magnetometer data 27

4.2: Estimates of first six states for Bar Magnet magnetic field 29

4.3: Estimates of last six states for Bar Magnet magnetic field 30

4.4: Estimates of the projectile states for Rectangular Loop magnetic field 33

4.5: Estimates of Projectile States with 10^{-4}% sensor noise with Bar Magnet magnetic field 36

4.6 Estimates of Projectile States with 0.1% sensor noise with Rectangular Loop magnetic field 39

4.7: Variation of Error in Estimate with Sensor Noise 41

4.8: Variation of Error in Estimation of State Values at Low Noise Levels 42

4.9: Variation of Final Error with Data Burst Length with magnetometer readings corrupted by 0.03% Noise 43

4.10: Variation of Final Error with Data Burst Length with accurate magnetometer sensor readings 44

LIST OF FIGURES (continued)

Figure Page

4.11: VARIATION OF FINAL ERROR WITH NUMBER OF MAGNETOMETER SENSORS 46

INITIAL STATE ESTIMATION FOR A GUN LAUNCHED PROJECTILE IN A SPATIALLY VARYING MAGNETIC FIELD

1. INTRODUCTION

1.1. Outline

Gun launched projectiles provide a significant challenge for the problem of navigation. Unlike aircrafts and missiles, whose initial conditions can be specified by the firing platform, the initial conditions for gun launched projectiles cannot be adequately specified, due to the inherent uncertainty in shot-to-shot launching conditions.

Smart weapons or Precision Guided Munitions are weapons that can be aimed or directed against a single target, relying on their own guidance systems. One of the most critical components of a smart weapon system is its sensor suite that provides position, orientation, and velocity information as the projectile flies down range so that effective control action can be taken in flight. Great strides have been made in creating very small and rugged Inertial Measurement Units (IMU) using MEMS

accelerometers and vibrating gyroscopes. However, all IMU systems operate by integrating accelerometer and gyroscope measurements. Thus, they must be initialized at launch to produce sufficiently accurate position and orientation data. Currently, there is no adequate method to initialize IMU sensor suites on gun launched munitions.

This thesis investigates a novel concept for determining the full state of a projectile near the muzzle of the gun. The methodology relies on the gun system inducing a known spatially varying magnetic field in the vicinity of the muzzle of the gun. Using readings from a cluster of magnetometers embedded within the projectile, the full state of the projectile is determined by solving a nonlinear set of equations.

1.2. Organization of the Thesis

Chapter 2 provides the background of this thesis. It briefly explains the motivation behind the initial state estimation problem. Chapter 3 describes the mathematical model of the system and develops the relationship between sensor readings and the projectile state. Chapter 4 presents the results of the MATLAB simulation for various different conditions. Chapter 5 discusses the results of the simulations and presents the scope for future work in the initial state estimation problem.

2. BACKGROUND

2.1. Smart Weapon Systems

Smart Weapons or Precision Guided Munitions provide a leap-ahead capability in terms of accuracy and engagement range for medium and large caliber projectiles. They are weapons that can be aimed at a target based on their own guidance systems. Smart weapons can be launched from aircrafts, ships, submarines, land vehicles or even by individual soldiers on ground [6].

Typically, smart weapons have two components – the Guidance Unit and the Control Unit. The guidance unit consists of a sensor which senses energy originating from the source or target destination. The control unit controls the flight of the projectile from the source to the target.

2.2. Inertial Navigation for Smart Weapons

Inertial navigation is the most accepted solution for guidance of smart weapons in military navigation applications, since it does not need any external aid or references. It can work anywhere and can operate autonomous, without using antennas or producing signatures. Thus, it can not be disturbed or manipulated by external sources.

However, errors in inertial navigation grow with time and inertial navigation sensors require a significant calibration effort before operation. It has been shown that a combination of GPS receivers and IMU sensors can be used to determine accurate position, velocity and attitude information of a projectile in flight, if the pre-launch calibration of IMU sensors is done accurately [10]. But, the initialization of inertial navigation sensors can not be done before launch, since the launch shock changes sensor errors unpredictably. Thus, inertial sensor calibration has to be done in flight [9].

Inertial navigation is based on *inertial sensors*. There are many types of inertial sensors for use with smart weapons, such as accelerometers, gyroscopes, magnetometers and inertial measurement unit sensors [2]. *Accelerometers* measure the acceleration of a point relative to the ground. *Gyroscopes* measure the angular velocity vector of the projectile with respect to the ground. *Magnetometers* measure the dot product between the magnetic field vector and the sensitive axis of the magnetometer at a particular point. They do not measure any rigid projectile model states directly, and require processing to obtain useful sensor feedback data. The *Inertial Measurement Unit Sensors* are multi-sensors that utilize three orthogonal accelerometers and three orthogonal gyroscopes. They use projectile kinematic differential equations to obtain state estimates. However, since estimates are obtained

by a numerical solution of a nonlinear differential equation, the initial conditions must be supplied to the sensor.

Magnetometer sensors have been used in navigation since centuries. Advances in technology have led to solid state electronic compasses, based on the original magnetic compasses used by sailors. Electronic compasses offer many advantages over conventional needle type or gimballed magnetic compasses, such as shock and vibration resistance, electronic compensation for stray field effects, and direct interface to electronic navigation systems [3]. They can be used to sense the strength and direction of magnetic field generated not only from the Earth, but also from permanent magnets, magnetized magnets, and fields generated form electric currents. Thus, magnetic sensors are being used with many navigation control systems.

3. INITIAL STATE ESTIMATION

This chapter suggests a solution to the problem of initial state estimation. It describes the rigid body model for a projectile and develops the equations of motion for a magnetometer sensor system. It then suggests a solution to the initial state estimation problem using the Enhanced Newton Method and Nonlinear Regression.

3.1. Rigid Body Model of Projectile

The definition of the position and orientation of a 6 Degree Of Freedom (DOF) projectile with sensors is aided by three main reference frames defined as follows

- I-frame: The ground is used as an inertial reference frame. It is fixed to the surface of earth and situated such that $\vec{I}_I - \vec{J}_I$ are in the plane of ground and $\vec{K}_I$ points down.
- B-frame: The body frame is located at the projectile mass center. It is fixed such that $\vec{I}_B$ points out of the nose of the projectile and $\vec{J}_B - \vec{K}_B$ form a right handed system.
- S-frame: The sensor frame is fixed on the rigid body and aligned with a sensor. The sensor frame is defined such that the outputs of the ith sensor are along $\vec{I}_{Si}, \vec{J}_{Si}, \vec{K}_{Si}$.

Figure 3.1 shows the geometry of a projectile with respect to these three reference frames. Inertial Frame is fixed to surface of the earth, Body Frame is centered at the Center of Gravity of the projectile and Sensor Frame is centered at the Center of Gravity of the sensor, which is placed on the projectile.

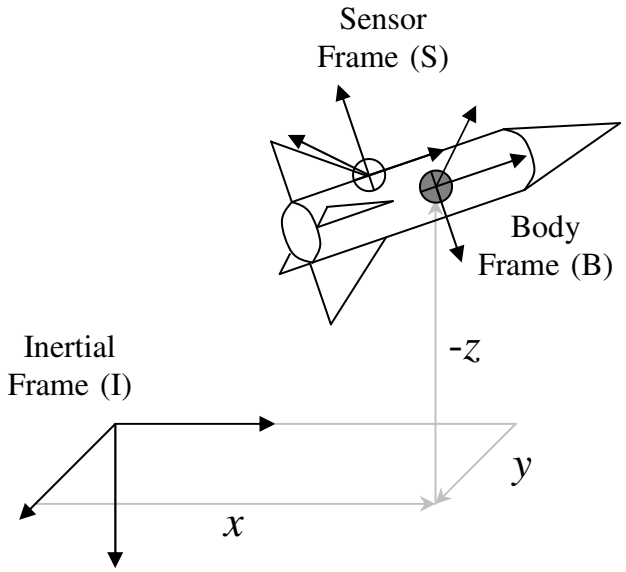

Figure 3.1: Projectile Geometry with respect to Inertial, Body and Sensor Reference Frames

The rigid body model of a projectile can be defined by using components of the position vector of mass center in inertial reference frame (x, y, z) and body orientation Euler angles (ϕ, θ, ψ). Figure 3.2 shows the geometry of the projectile with respect to

orientation of the projectile in the inertial frame, with Euler roll (ϕ), pitch (θ) and yaw (ψ) angles.

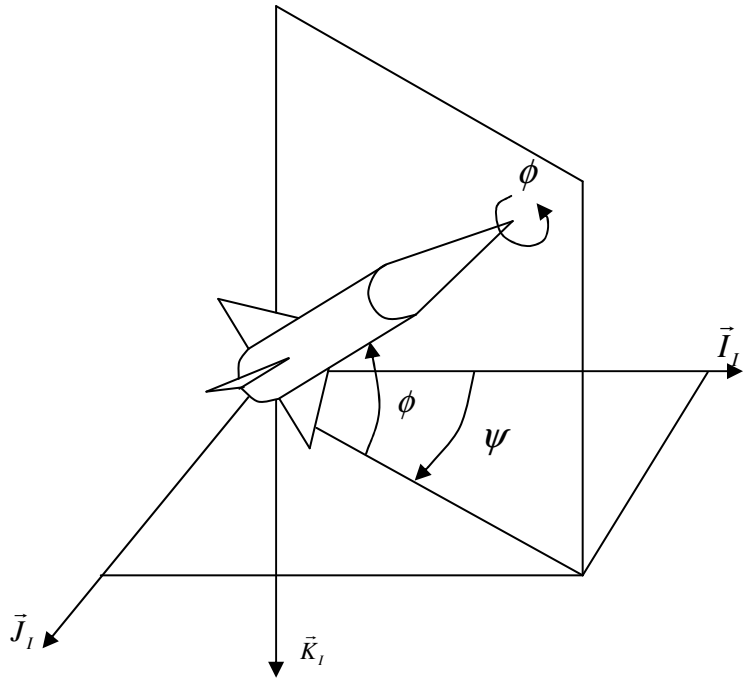

Figure 3.2: Euler Angle Geometry of a Projectile with respect to Inertial Frame

3.2. Reference Frame Relationships

The Inertial Reference Frame and Body Reference Frame are related by a sequence of three single-axis Body Fixed Rotations. Starting with the Inertial frame and rotating through angle ψ about axis $\vec{K}_I$ generates *Intermediate Frame 1*. Rotating this frame through an angle θ about the axis $\vec{J}_1$ generates the *No Roll Frame (NR)*. Rotating NR

through an angle ϕ about the axis $\vec{I}_{NR}$ generates the Body Frame (B). These rotations can be expressed mathematically as shown in equations (3.2.1) – (3.2.3).

$$\begin{Bmatrix} \vec{I}_1 \\ \vec{J}_1 \\ \vec{K}_1 \end{Bmatrix} = \begin{bmatrix} \cos\psi & \sin\psi & 0 \\ -\sin\psi & \cos\psi & 0 \\ 0 & 0 & 1 \end{bmatrix} \begin{Bmatrix} \vec{I}_I \\ \vec{J}_I \\ \vec{K}_I \end{Bmatrix} \tag{3.2.1}$$

$$\begin{Bmatrix} \vec{I}_{NR} \\ \vec{J}_{NR} \\ \vec{K}_{NR} \end{Bmatrix} = \begin{bmatrix} \cos\theta & 0 & -\sin\theta \\ 0 & 1 & 0 \\ \sin\theta & 0 & \cos\theta \end{bmatrix} \begin{Bmatrix} \vec{I}_1 \\ \vec{J}_1 \\ \vec{K}_1 \end{Bmatrix} \tag{3.2.2}$$

$$\begin{Bmatrix} \vec{I}_B \\ \vec{J}_B \\ \vec{K}_B \end{Bmatrix} = \begin{bmatrix} 1 & 0 & 0 \\ 0 & \cos\phi & \sin\phi \\ 0 & -\sin\phi & \cos\phi \end{bmatrix} \begin{Bmatrix} \vec{I}_{NR} \\ \vec{J}_{NR} \\ \vec{K}_{NR} \end{Bmatrix} \tag{3.2.3}$$

The three equations can be combined together to generate the equation for the transformation between the Inertial Frame and the Body Frame shown in equation (3.2.4)

$$\begin{Bmatrix} \vec{I}_B \\ \vec{J}_B \\ \vec{K}_B \end{Bmatrix} = \begin{bmatrix} c_\theta c_\varphi & c_\theta s_\varphi & -s_\theta \\ s_\phi s_\theta c_\varphi - c_\phi s_\psi & s_\phi s_\theta s_\varphi + c_\phi c_\varphi & s_\phi c_\theta \\ c_\phi s_\theta c_\varphi + s_\phi s_\psi & c_\phi s_\theta s_\varphi - s_\phi c_\psi & c_\phi c_\theta \end{bmatrix} \begin{bmatrix} \vec{I}_I \\ \vec{J}_I \\ \vec{K}_I \end{bmatrix} = [T_B] \begin{Bmatrix} \vec{I}_I \\ \vec{J}_I \\ \vec{K}_I \end{Bmatrix} \tag{3.2.4}$$

Similarly, the transformation between the Body Frame and Sensor Frame is given by equation (3.2.5)

$$\begin{Bmatrix} \vec{I}_{Si} \\ \vec{J}_{Si} \\ \vec{K}_{Si} \end{Bmatrix} = [T_{Si}] \begin{Bmatrix} \vec{I}_{B} \\ \vec{J}_{B} \\ \vec{K}_{B} \end{Bmatrix} \tag{3.2.5}$$

3.3. Projectile State Variables

A rigid projectile has six degrees of freedom. Since each degree of freedom generates a second order differential equation, the model requires 12 state variables. The full state of the projectile is given by equation (3.3.1).

$$\vec{\xi} = \begin{Bmatrix} x \\ y \\ z \\ \phi \\ \theta \\ \psi \\ u \\ v \\ w \\ p \\ q \\ r \end{Bmatrix} \tag{3.3.1}$$

where,

x, y, z = Components of position vector of the mass center in an inertial frame.

ϕ, θ, ψ = Euler roll, pitch and yaw angles.

u, v, w = Components of velocity vector of the mass center in an inertial frame.

p, q, r = Components of angular velocity of the system in the body reference frame.

The velocity vector definition for a rigid body is given in equations (3.3.2) and (3.3.3).

$$\vec{V}_{CG/I} = \dot{x}\vec{I}_I + \dot{y}\vec{J}_I + \dot{z}\vec{K}_I \tag{3.3.2}$$

$$\vec{V}_{CG/I} = u\vec{I}_B + v\vec{J}_B + w\vec{K}_B \tag{3.3.3}$$

Comparing, equations (3.3.2) and equation (3.3.3) using equation (3.2.4), we can write equation (3.3.4)

$$\begin{Bmatrix} \dot{x} \\ \dot{y} \\ \dot{z} \end{Bmatrix} = \begin{bmatrix} c_\theta c_\psi & s_\phi s_\theta c_\psi - c_\phi s_\psi & c_\phi s_\theta c_\psi + s_\phi s_\psi \\ c_\theta s_\psi & s_\phi s_\theta s_\psi + c_\phi c_\psi & c_\phi s_\theta s_\psi - s_\phi c_\psi \\ -s_\theta & s_\phi c_\theta & c_\phi c_\theta \end{bmatrix} \begin{Bmatrix} u \\ v \\ w \end{Bmatrix} \tag{3.3.4}$$

Similarly the definition of angular velocity for a rigid body is given by equations (3.3.5) and (3.3.6).

$$\vec{\omega}_{B/I} = \dot{\psi}\vec{K}_I + \dot{\theta}\vec{J}_1 + \dot{\phi}\vec{I}_{NR} \tag{3.3.5}$$

$$\vec{\omega}_{B/I} = p\vec{I}_B + q\vec{J}_B + r\vec{K}_B \tag{3.3.6}$$

Comparing equations (3.3.5) and (3.3.6) using equation (3.2.4), we can write equation (3.3.7)

$$\begin{Bmatrix} \dot{\phi} \\ \dot{\theta} \\ \dot{\psi} \end{Bmatrix} = \begin{bmatrix} 1 & s_\phi t_\theta & c_\phi t_\theta \\ 0 & c_\phi & -s_\phi \\ 0 & s_\phi / c_\theta & c_\phi / c_\theta \end{bmatrix} \begin{Bmatrix} p \\ q \\ r \end{Bmatrix} \tag{3.3.7}$$

Equations (3.3.4) and (3.3.7) are the *Kinematic Differential Equations* of the projectile.

3.4. Magnetometer Sensor Readings

Near the muzzle of the gun, it is assumed that a magnetic field is generated that is a function of the spatial position of the sensor. It is most easily defined in the ground frame (I-frame).

$$\vec{e}_A = e_x(\vec{r}_{O\to A})\vec{I}_I + e_y(\vec{r}_{O\to A})\vec{J}_I + e_z(\vec{r}_{O\to A})\vec{K}_I \tag{3.4.1}$$

where, $\vec{e}_A$ is the magnetic field at point A in space.

The magnetic field experienced by a magnetometer moving in space is given by

$$\vec{e}_{Si} = \vec{e}_{Si}(\vec{r}_{O\to A}) = e_{xi}(x_i, y_i, z_i)\vec{I}_I + e_{yi}(x_i, y_i, z_i)\vec{J}_I + e_{iz}(x_i, y_i, z_i)\vec{K}_I \tag{3.4.2}$$

For an ideal magnetometer, the components of the magnetic field are recorded in the S_i reference frame.

$$\vec{e}_{Si} = m_{xi}(x_i, y_i, z_i)\vec{I}_{Si} + m_{yi}(x_i, y_i, z_i)\vec{J}_{Si} + m_{zi}(x_i, y_i, z_i)\vec{K}_{Si} \tag{3.4.3}$$

Equating expressions of $\vec{e}_{Si}$ from equations (3.4.2) and (3.4.3) in frame S_i yields

$$\begin{Bmatrix} m_{xi} \\ m_{yi} \\ m_{zi} \end{Bmatrix} = [T_{Si}][T_B]\begin{Bmatrix} e_{xi} \\ e_{yi} \\ e_{zi} \end{Bmatrix} \tag{3.4.4}$$

$$\begin{Bmatrix} \dot{m}_{xi} \\ \dot{m}_{yi} \\ \dot{m}_{zi} \end{Bmatrix} = [T_{Si}]\left[\dot{T}_B\right]\begin{Bmatrix} e_{xi} \\ e_{yi} \\ e_{zi} \end{Bmatrix} + [T_{Si}][T_B]\begin{Bmatrix} \dot{e}_{xi} \\ \dot{e}_{yi} \\ \dot{e}_{zi} \end{Bmatrix} \tag{3.4.5}$$

Like all sensors, real magnetometers experience errors such as noise, bias, cross axis sensitivity and scale factor. Thus a real magnetometer output takes the form

$$\begin{Bmatrix} \tilde{m}_{xi} \\ \tilde{m}_{yi} \\ \tilde{m}_{zi} \end{Bmatrix} = \begin{Bmatrix} n_{xi} \\ n_{yi} \\ n_{zi} \end{Bmatrix} + \begin{Bmatrix} b_{xi} \\ b_{yi} \\ b_{zi} \end{Bmatrix} + \begin{bmatrix} s_{xxi} & c_{xyi} & c_{xzi} \\ c_{yxi} & s_{yyi} & c_{yzi} \\ c_{zxi} & c_{zyi} & s_{zzi} \end{bmatrix}\begin{Bmatrix} m_{xi} \\ m_{yi} \\ m_{zi} \end{Bmatrix} \tag{3.4.6}$$

Which, from equation (3.4.4) is equivalent to

$$\begin{Bmatrix} \tilde{m}_{xi} \\ \tilde{m}_{yi} \\ \tilde{m}_{zi} \end{Bmatrix} = \begin{Bmatrix} n_{xi} \\ n_{yi} \\ n_{zi} \end{Bmatrix} + \begin{Bmatrix} b_{xi} \\ b_{yi} \\ b_{zi} \end{Bmatrix} + \begin{bmatrix} s_{xxi} & c_{xyi} & c_{xzi} \\ c_{yxi} & s_{yyi} & c_{yzi} \\ c_{zxi} & c_{zyi} & s_{zzi} \end{bmatrix}[T_{Si}][T_B]\begin{Bmatrix} e_{xi} \\ e_{yi} \\ e_{zi} \end{Bmatrix} \tag{3.4.7}$$

And,

$$\begin{Bmatrix} \dot{\tilde{m}}_{xi} \\ \dot{\tilde{m}}_{yi} \\ \dot{\tilde{m}}_{zi} \end{Bmatrix} = \begin{Bmatrix} \dot{n}_{xi} \\ \dot{n}_{yi} \\ \dot{n}_{zi} \end{Bmatrix} + \begin{bmatrix} s_{xxi} & c_{xyi} & c_{xzi} \\ c_{yxi} & s_{yyi} & c_{yzi} \\ c_{zxi} & c_{zyi} & s_{zzi} \end{bmatrix} \left[[T_{Si}] \left[\dot{T}_B \right] \begin{Bmatrix} e_{xi} \\ e_{yi} \\ e_{zi} \end{Bmatrix} + [T_{Si}][T_B] \begin{Bmatrix} \dot{e}_{xi} \\ \dot{e}_{yi} \\ \dot{e}_{zi} \end{Bmatrix} \right] \quad (3.4.8)$$

We shall now generate an expression for $\dot{T}_B$. From equation (3.2.4), we have

$$\begin{Bmatrix} \vec{I}_B \\ \vec{J}_B \\ \vec{K}_B \end{Bmatrix} = [T_B] \begin{Bmatrix} \vec{I}_I \\ \vec{J}_I \\ \vec{K}_I \end{Bmatrix} \Rightarrow \begin{Bmatrix} \vec{I}_I \\ \vec{J}_I \\ \vec{K}_I \end{Bmatrix} = [T_B]^T \begin{Bmatrix} \vec{I}_B \\ \vec{J}_B \\ \vec{K}_B \end{Bmatrix} \quad (3.4.9)$$

Also, note that

$$^I \frac{d\vec{I}_B}{dt} = \dot{T}_{B11} \vec{I}_I + \dot{T}_{B12} \vec{J}_I + \dot{T}_{B13} \vec{K}_I$$

$$^I \frac{d\vec{J}_B}{dt} = \dot{T}_{B21} \vec{I}_I + \dot{T}_{B22} \vec{J}_I + \dot{T}_{B23} \vec{K}_I$$

$$^I \frac{d\vec{K}_B}{dt} = \dot{T}_{B31} \vec{I}_I + \dot{T}_{B32} \vec{J}_I + \dot{T}_{B33} \vec{K}_I$$

$$\Rightarrow \begin{Bmatrix} ^I \frac{d\vec{I}_B}{dt} \\ ^I \frac{d\vec{J}_B}{dt} \\ ^I \frac{d\vec{K}_B}{dt} \end{Bmatrix} = \left[\dot{T}_B \right] \begin{Bmatrix} \vec{I}_I \\ \vec{J}_I \\ \vec{K}_I \end{Bmatrix} = \left[\dot{T}_B \right] [T_B]^T \begin{Bmatrix} \vec{I}_B \\ \vec{J}_B \\ \vec{K}_B \end{Bmatrix} \quad (3.4.10)$$

Using the frame derivative relationship,

$$ {}^{I}\frac{dI_B}{dt} = {}^{B}\frac{dI_B}{dt} + \vec{\omega}_{B/I} x \vec{I}_B = (p\vec{I}_B + q\vec{J}_B + r\vec{K}_B) x \vec{I}_B $$

$$ {}^{I}\frac{d\vec{I}_B}{dt} = r\vec{J}_B - q\vec{K}_B \tag{3.4.11} $$

Similarly,

$$ {}^{I}\frac{d\vec{J}_B}{dt} = -r\vec{I}_B + p\vec{K}_B \tag{3.4.12} $$

$$ {}^{I}\frac{d\vec{K}_B}{dt} = q\vec{I}_B - p\vec{J}_B \tag{3.4.13} $$

Therefore,

$$ \begin{Bmatrix} {}^{I}\frac{d\vec{I}_B}{dt} \\ {}^{I}\frac{d\vec{J}_B}{dt} \\ {}^{I}\frac{d\vec{K}_B}{dt} \end{Bmatrix} = \begin{bmatrix} 0 & r & -q \\ -r & 0 & p \\ q & -p & 0 \end{bmatrix} \begin{Bmatrix} \vec{I}_B \\ \vec{J}_B \\ \vec{K}_B \end{Bmatrix} \tag{3.4.14} $$

Equating expressions (3.4.10) and (3.4.14),

$$ \begin{bmatrix} \dot{T}_B \end{bmatrix} = -\begin{bmatrix} 0 & -r & q \\ r & 0 & -p \\ -q & p & 0 \end{bmatrix} \begin{bmatrix} T_B \end{bmatrix} \tag{3.4.15} $$

Since e_{xi} , e_{yi} and e_{zi} are functions of quantities x_i, y_i and z_i,

$$\dot{e}_{xi} = \frac{\partial e_{xi}}{\partial x_i}\dot{x}_i + \frac{\partial e_{xi}}{\partial y_i}\dot{y}_i + \frac{\partial e_{xi}}{\partial z_i}\dot{z}_i \tag{3.4.16}$$

$$\dot{e}_{yi} = \frac{\partial e_{yi}}{\partial x_i}\dot{x}_i + \frac{\partial e_{yi}}{\partial y_i}\dot{y}_i + \frac{\partial e_{yi}}{\partial z_i}\dot{z}_i \tag{3.4.17}$$

$$\dot{e}_{zi} = \frac{\partial e_{zi}}{\partial x_i}\dot{x}_i + \frac{\partial e_{zi}}{\partial y_i}\dot{y}_i + \frac{\partial e_{zi}}{\partial z_i}\dot{z}_i \tag{3.4.18}$$

$$\begin{Bmatrix} \dot{e}_{xi} \\ \dot{e}_{yi} \\ \dot{e}_{zi} \end{Bmatrix} = \begin{bmatrix} \frac{\partial e_{xi}}{\partial x_i} & \frac{\partial e_{xi}}{\partial y_i} & \frac{\partial e_{xi}}{\partial z_i} \\ \frac{\partial e_{yi}}{\partial x_i} & \frac{\partial e_{yi}}{\partial x_i} & \frac{\partial e_{yi}}{\partial x_i} \\ \frac{\partial e_{xi}}{\partial x_i} & \frac{\partial e_{xi}}{\partial x_i} & \frac{\partial e_{xi}}{\partial x_i} \end{bmatrix} \begin{Bmatrix} \dot{x}_i \\ \dot{y}_i \\ \dot{z}_i \end{Bmatrix} = [J_E] \begin{Bmatrix} \dot{x}_i \\ \dot{y}_i \\ \dot{z}_i \end{Bmatrix} \tag{3.4.19}$$

The position of the ith magnetometer is related to the mass center position by the following equation

$$\begin{Bmatrix} x_i \\ y_i \\ z_i \end{Bmatrix} = \begin{Bmatrix} x \\ y \\ z \end{Bmatrix} + [T_B]^T \begin{Bmatrix} \Delta SL_i \\ \Delta BL_i \\ \Delta WL_i \end{Bmatrix} \tag{3.4.20}$$

where,

$$\vec{r}_{O\to CG} = x\vec{I}_I + y\vec{J}_I + z\vec{K}_I$$

$$\vec{r}_{CG\to i} = \Delta SL_i\vec{I}_B + \Delta BL_i\vec{J}_B + \Delta WL_i\vec{K}_B$$

Taking a derivative of this expression yields

$$\begin{Bmatrix} \dot{x}_i \\ \dot{y}_i \\ \dot{z}_i \end{Bmatrix} = \begin{Bmatrix} \dot{x} \\ \dot{y} \\ \dot{z} \end{Bmatrix} + \left[\dot{T}_B\right]^T \begin{Bmatrix} \Delta SL_i \\ \Delta BL_i \\ \Delta WL_i \end{Bmatrix} \tag{3.4.21}$$

Using rotational kinematic equation (3.3.4) and equation (3.4.15) we get

$$\begin{Bmatrix} \dot{x}_i \\ \dot{y}_i \\ \dot{z}_i \end{Bmatrix} = \left[T_B\right]^T \left[\begin{Bmatrix} u \\ v \\ w \end{Bmatrix} + \begin{bmatrix} 0 & -r & q \\ r & 0 & -p \\ -q & p & 0 \end{bmatrix} \begin{Bmatrix} \Delta SL_i \\ \Delta BL_i \\ \Delta WL_i \end{Bmatrix} \right] \tag{3.4.22}$$

Re-expressing the ideal magnetometer equations,

$$\begin{Bmatrix} m_{xi} \\ m_{yi} \\ m_{zi} \end{Bmatrix} = \left[T_{Si}\right]\left[T_B\right] \begin{Bmatrix} e_{xi} \\ e_{yi} \\ e_{zi} \end{Bmatrix} \tag{3.4.23}$$

$$\begin{Bmatrix} \dot{m}_{xi} \\ \dot{m}_{yi} \\ \dot{m}_{zi} \end{Bmatrix} = -\left[T_{Si}\right] \begin{bmatrix} 0 & -r & q \\ r & 0 & -p \\ -q & p & 0 \end{bmatrix} \left[T_B\right] \begin{Bmatrix} e_{xi} \\ e_{yi} \\ e_{zi} \end{Bmatrix} + \left[T_{Si}\right]\left[T_B\right]\left[J_E\right]\left[T_B\right]^T \left[\begin{Bmatrix} u \\ v \\ w \end{Bmatrix} + \begin{bmatrix} 0 & -r & q \\ r & 0 & -p \\ -q & p & 0 \end{bmatrix} \begin{Bmatrix} \Delta SL_i \\ \Delta BL_i \\ \Delta WL_i \end{Bmatrix} \right] \tag{3.4.24}$$

Substituting equation (3.4.23) into equation (3.4.24),

$$\begin{Bmatrix} \dot{m}_{xi} \\ \dot{m}_{yi} \\ \dot{m}_{zi} \end{Bmatrix} = -[T_{Si}] \begin{bmatrix} 0 & -r & q \\ r & 0 & -p \\ -q & p & 0 \end{bmatrix} [T_{Si}]^T \begin{Bmatrix} m_{xi} \\ m_{yi} \\ m_{zi} \end{Bmatrix} + [T_{Si}][T_B][J_E][T_B]^T \left[\begin{Bmatrix} u \\ v \\ w \end{Bmatrix} + \begin{bmatrix} 0 & -r & q \\ r & 0 & -p \\ -q & p & 0 \end{bmatrix} \begin{Bmatrix} \Delta SL_i \\ \Delta BL_i \\ \Delta WL_i \end{Bmatrix} \right]$$

(3.4.25)

Thus the full state of the rigid projectile is contained in the magnetometer and magnetometer derivative expressions.

The translational velocity components (u, v, w) and the angular rate components (p, q, r) are present in the time derivatives of the magnetometer readings. Thus, in order for the translational velocity components to be contained in $\dot{m}_{xi}$, $\dot{m}_{yi}$ and $\dot{m}_{zi}$ the magnetic field around the muzzle of the gun must be spatially varying. If the magnetic field is constant in the area around the gun muzzle, then the matrix J_E is zero and the dependence of $\dot{m}_{xi}$, $\dot{m}_{yi}$ and $\dot{m}_{zi}$ on u, v and w is eliminated. However, the angular rate components p, q and r appear twice; once with the magnetic field component having a spatially varying nature, and once without it. Thus p, q and r are present in $\dot{m}_{xi}$, $\dot{m}_{yi}$ and $\dot{m}_{zi}$ even when the magnetic field is spatially constant.

3.5. Projectile Initial State Estimation

A spatially varying and known magnetic field is set up near the gun muzzle. This magnetic field is sampled by the magnetometers that pass through the field. It is assumed that an array of magnetometers mounted on the projectile records a finite sample of measurements in the area around the muzzle of the gun. The problem is split into two parts – estimating the first six states of the projectile, and then using Projectile Kinematic Equations to find the last six states.

3.5.1. Enhanced Newton's Method

To solve the first part of this problem, consider the magnetometer equation given in equation (3.4.23). Given the magnetometer data at some time, and an estimate of the states, the residual of these equations is computed.

$$\begin{Bmatrix} f_{mxi} \\ f_{myi} \\ f_{mzi} \end{Bmatrix} = \begin{Bmatrix} m_{xi} \\ m_{yi} \\ m_{zi} \end{Bmatrix} - [T_{Si}][T_B(\phi,\theta,\varphi)] \begin{Bmatrix} e_{xi} \\ e_{yi} \\ e_{zi} \end{Bmatrix} \tag{3.5.1}$$

where f_{mx}, f_{my}, f_{mz}, are the equation residuals. If N tri-axial magnetometers are mounted on the projectile, the residual vector is defined in the following manner.

$$F = \{F_m\} \tag{3.5.2}$$

where,

$$F_m = \begin{Bmatrix} f_{mx1} \\ f_{my1} \\ f_{mz1} \\ \hline f_{mx2} \\ f_{my2} \\ f_{mz2} \\ \vdots \\ \hline f_{mxn} \\ f_{myn} \\ f_{mzn} \end{Bmatrix}$$

The goal of the estimation procedure is to find the state vector $X = [x \quad y \quad z \quad \phi \quad \theta \quad \psi]$ such that F_m is sufficiently close to zero. A nonlinear least squares procedure is used for this purpose where a merit function defined below is minimized.

$$J = \frac{1}{2} F^T W F \tag{3.5.3}$$

Note that W is a positive definite symmetric matrix. To minimize the merit function, it is approximated as a quadratic function in the initial projectile state vector.

$$J(X) \cong J_0 + \frac{\partial J}{\partial X}\Big|_{xo} (X - X_o) + \frac{1}{2}(X - X_o)^T \frac{\partial^2 J}{\partial X^2}\Big|_{xo} (X - X_o) \tag{3.5.4}$$

where,

$$J_o = \frac{1}{2} F^T(X_o) W F(X_o)$$

$$\frac{\partial J}{\partial X} = \begin{bmatrix} \frac{\partial J}{\partial x} & \frac{\partial J}{\partial y} & \cdots & \frac{\partial J}{\partial \psi} \end{bmatrix}$$

Now,

$$\frac{\partial J}{\partial X} = \left(\frac{\partial F}{\partial X}\right)^T \frac{\partial J}{\partial F} = \left(\frac{\partial F}{\partial X}\right)^T W F \tag{3.5.5}$$

And,

$$\frac{\partial^2 J}{\partial X^2} = \begin{bmatrix} \frac{\partial}{\partial x}\left(\frac{\partial J}{\partial x}\right) & \frac{\partial}{\partial y}\left(\frac{\partial J}{\partial x}\right) & \cdots & \frac{\partial}{\partial r}\left(\frac{\partial J}{\partial x}\right) \\ \frac{\partial}{\partial x}\left(\frac{\partial J}{\partial y}\right) & \frac{\partial}{\partial y}\left(\frac{\partial J}{\partial y}\right) & \cdots & \frac{\partial}{\partial r}\left(\frac{\partial J}{\partial y}\right) \\ \vdots & \vdots & \ddots & \vdots \\ \frac{\partial}{\partial x}\left(\frac{\partial J}{\partial \psi}\right) & \frac{\partial}{\partial y}\left(\frac{\partial J}{\partial \psi}\right) & \cdots & \frac{\partial}{\partial r}\left(\frac{\partial J}{\partial \psi}\right) \end{bmatrix} \tag{3.5.6}$$

$$\frac{\partial^2 J}{\partial X^2} = \left[\frac{\partial}{\partial x_1}\left[\left(\frac{\partial F}{\partial X}\right)^T\right] WF \vdots \quad \frac{\partial}{\partial x_2}\left[\left(\frac{\partial F}{\partial X}\right)^T\right] WF \vdots \quad \cdots \quad \vdots \frac{\partial}{\partial x_N}\left[\left(\frac{\partial F}{\partial X}\right)^T\right] WF \right] + \left(\frac{\partial F}{\partial X}\right)^T W \left(\frac{\partial F}{\partial X}\right) \tag{3.5.7}$$

Solving for X to force $\frac{\partial J}{\partial X}$=0,

$$\frac{\partial J}{\partial X}\Big|_{xo} + \frac{\partial^2 J}{\partial X^2}(X - X_o) = 0$$

Or,

$$\{X\} = \{X_0\} - \left[\frac{\partial^2 J}{\partial X^2}\right]^{-1}_{xo} \left\{\frac{\partial J}{\partial X}\right\}_{xo} \tag{3.5.8}$$

Since our nonlinear equations are not perfectly modeled by a quadratic, we iteratively perform this operation until convergence.

$$\{X\}_{i+1} = \{X\}_i - \left[\frac{\partial^2 J}{\partial X^2}\right]^{-1} \left\{\frac{\partial J}{\partial X}\right\} \tag{3.5.9}$$

Furthermore, the nonlinear equations can be so poorly modeled by a quadratic that a new point may actually generate a higher value of cost. To get around this, we use the *Enhanced Newton's Method*, where we alter the pure Newton's Method with a line search scalar parameter.

$$\{X\}_{i+1} = \{X\}_i - \alpha_i \left[\frac{\partial^2 J}{\partial X^2}\right]^{-1} \left\{\frac{\partial J}{\partial X}\right\} \tag{3.5.10}$$

where, α_i is a line search parameter and the term $\left[\frac{\partial^2 J}{\partial X^2}\right]^{-1}_i \left\{\frac{\partial J}{\partial X}\right\}$ gives the search direction.

The line search parameter is determined by a back stepping procedure in which α_i is assumed to be 1, at each iteration, to compute the next state. This new state is used to calculate the new cost function J_1. If $J_1 \leq \beta J_0$, then $\alpha_i = 1$ is accepted and the

process is repeated. On the other hand, if $J_1 > \beta J_0$, then α_i is set to α_i / k, and J_2 is computed. If $J_2 \leq \beta J_0$ then $\alpha_i = 1$ is accepted and the process is repeated.

3.5.2. Non Linear Regression

To solve the second part of the problem, we find the derivatives of the estimates of the first six states using *Non Linear Regression*, and use the Projectile Kinematic Equations to find the translational and angular velocity components of the state.

For finding the derivative of an estimated state, consider its estimate over several instances of time. For example, let us consider the estimate of state x over p instances of time. That is, the state vector $[x_1 \quad x_2 \quad \dots \quad x_p]$ corresponds to time instants $[t_1 \quad t_2 \quad \dots \quad t_p]$. We assume that the data is fit to an mth order polynomial, such that the following equations hold.

$$\begin{aligned} a_0 + a_1 t_1 + a_2 t_1^2 + \cdots + a_m t_1^m &= x_1 \\ a_0 + a_1 t_2 + a_2 t_2^2 + \cdots + a_m t_2^m &= x_2 \\ &\vdots \\ a_0 + a_1 t_p + a_2 t_p^2 + \cdots + a_m t_p^m &= x_p \end{aligned}$$

This can be written in matrix form as follows

$$\begin{bmatrix} 1 & t_1 & t_1^2 & \cdots & t_1^m \\ 1 & t_2 & t_2^2 & \cdots & t_2^m \\ \vdots & \vdots & \vdots & \ddots & \vdots \\ 1 & t_p & t_p^2 & \cdots & t_p^m \end{bmatrix} \begin{Bmatrix} a_0 \\ a_1 \\ a_2 \\ \vdots \\ a_m \end{Bmatrix} = \begin{Bmatrix} x_1 \\ x_2 \\ \vdots \\ x_p \end{Bmatrix} \tag{3.5.11}$$

Let,

$$B = \begin{bmatrix} 1 & t_1 & t_1^2 & \cdots & t_1^m \\ 1 & t_2 & t_2^2 & \cdots & t_2^m \\ \vdots & \vdots & \vdots & \ddots & \vdots \\ 1 & t_p & t_p^2 & \cdots & t_p^m \end{bmatrix}$$

$$A = \begin{Bmatrix} a_0 \\ a_1 \\ a_2 \\ \vdots \\ a_m \end{Bmatrix}$$

$$X = \begin{Bmatrix} x_1 \\ x_2 \\ \vdots \\ x_p \end{Bmatrix}$$

The equation can be rewritten as

$$BA = X \tag{3.5.12}$$

Equation (3.5.12) can be solved for the vector A to find the coefficients of the nonlinear equations. Since B is a rectangular matrix, we will have to use the *Least Mean Square* solution of equation (3.5.12) to solve for A.

Once the curve through a state is found, we can find its derivative as follows

$$\begin{aligned} & a_1 + 2a_2 t_1 + \cdots + m a_m t_1^{m-1} = \dot{x}_1 \\ & a_1 + 2a_2 t_2 + \cdots + m a_m t_2^{m-1} = \dot{x}_2 \\ & \vdots \\ & a_1 + 2a_1 t_p + \cdots + m a_m t_p^{m-1} = \dot{x}_p \end{aligned}$$

$$\Rightarrow \begin{bmatrix} 1 & 2t_1 & \cdots & m t_1^{m-1} \\ 1 & 2t_2 & \cdots & m t_2^{m-1} \\ \vdots & \vdots & \ddots & \vdots \\ 1 & 2t_p & \cdots & m t_p^{m-1} \end{bmatrix} \begin{Bmatrix} a_1 \\ a_2 \\ \vdots \\ a_m \end{Bmatrix} = \begin{Bmatrix} \dot{x}_1 \\ \dot{x}_2 \\ \vdots \\ \dot{x}_p \end{Bmatrix} \tag{3.5.13}$$

States u, v, w can be found by using derivatives of estimates of states x, y, z and the Projectile Kinematic Equation (3.3.4). Similarly, states p, q, r can be found by using the derivatives of estimated states ϕ, θ, ψ and Projectile Kinematic Equation (3.3.6).

4. IMPLEMENTATION AND RESULTS

Having suggested the solution to the Initial State Estimation problem, we now provide the empirical verification of the hypothesis. This chapter presents the results of the simulations and trade studies performed for different sensor geometries and magnetic fields. The simulations were performed using MATLABv7.0.4.

4.1. Experimental Setup and Procedure

In order to estimate the initial state of the projectile, magnetometer array sensor data has to be obtained. According to the methodology described in Chapter 3, sensor data for each sensor in the array is required over a period of time. The period of time over which this data is obtained, should be chosen carefully. It should be short enough to ensure linear variation of data, but long enough to generate enough number of samples for finding state derivatives.

For example, figure 4.1 shows the variation of sensor readings of a single magnetometer with time. We would like to select a sequence of as many points from this data set, as possible; since a greater number of points would generate more accurate state derivative estimates. However, if we pick the complete data set, nonlinearities in the data would prevent us from estimating state derivatives

accurately. Thus, we pick the data points enclosed by the red rectangle in the figure, to select a period which is almost linear and generates enough data points.

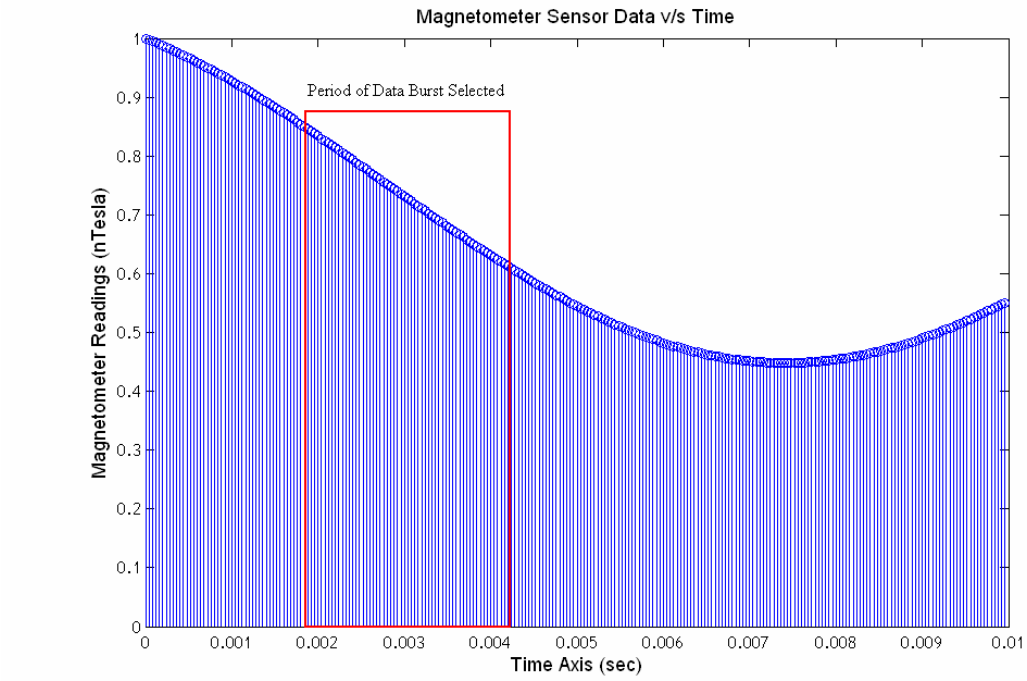

Figure 4.1: Selection of a data burst of a nonlinear sequence of magnetometer data

After an appropriate selection of magnetometer data is made, the first six states of the projectile are estimated at each data point, using the Enhanced Newton's Method as described in Section 3.5.1.

After the first six states are estimated at each time instant over the period of data burst, the next six states are determined using Nonlinear Regression, as described in Section 3.5.2.

Thus, an estimate of the full state is obtained by starting from magnetometer sensor readings.

4.2. State Estimation Without Sensor Noise

When there is no sensor noise, that is, each magnetometer in the sensor array measures the magnetic field accurately, the methodology works extremely well. The following sections show the results for a magnetic field generated by a current flowing through a a *bar magnet* and *a rectangular current carrying loop.*

4.2.1. Bar Magnet Magnetic Field

This section presents the results of state estimation when the projectile is traveling in a magnetic field generated by a bar magnet placed on the top of the muzzle of the launching gun. The magnetic field readings are obtained over 25 time steps by a sensor array having five magnetometers placed randomly on the projectile. The average of the final error over the 25 time steps is found to be $2.88\times10^{-4}\%$ of the actual values. The graphical results are as shown in figures 4.2 and 4.3.

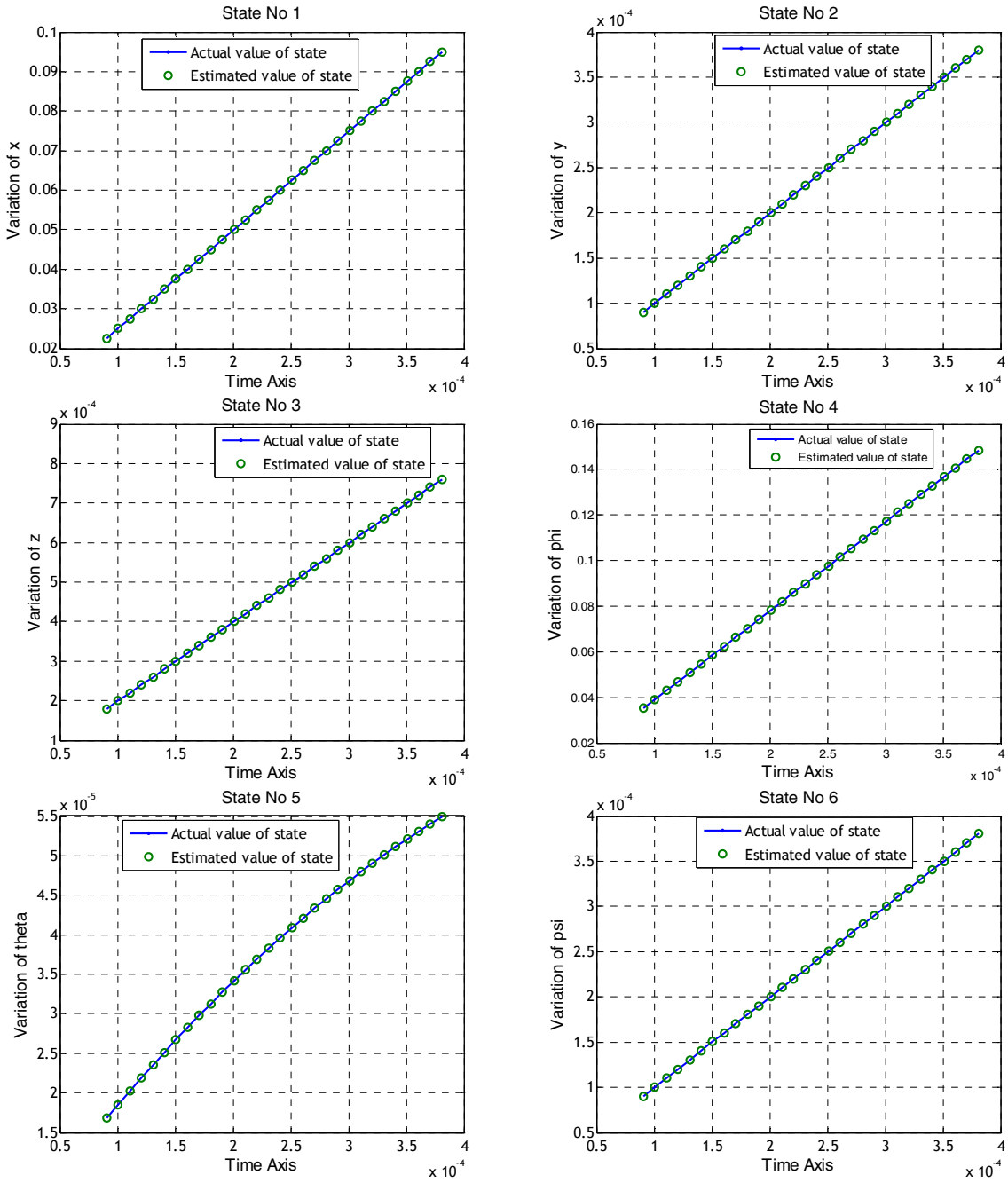

Figure 4.2: Estimates of first six states for Bar Magnet magnetic field

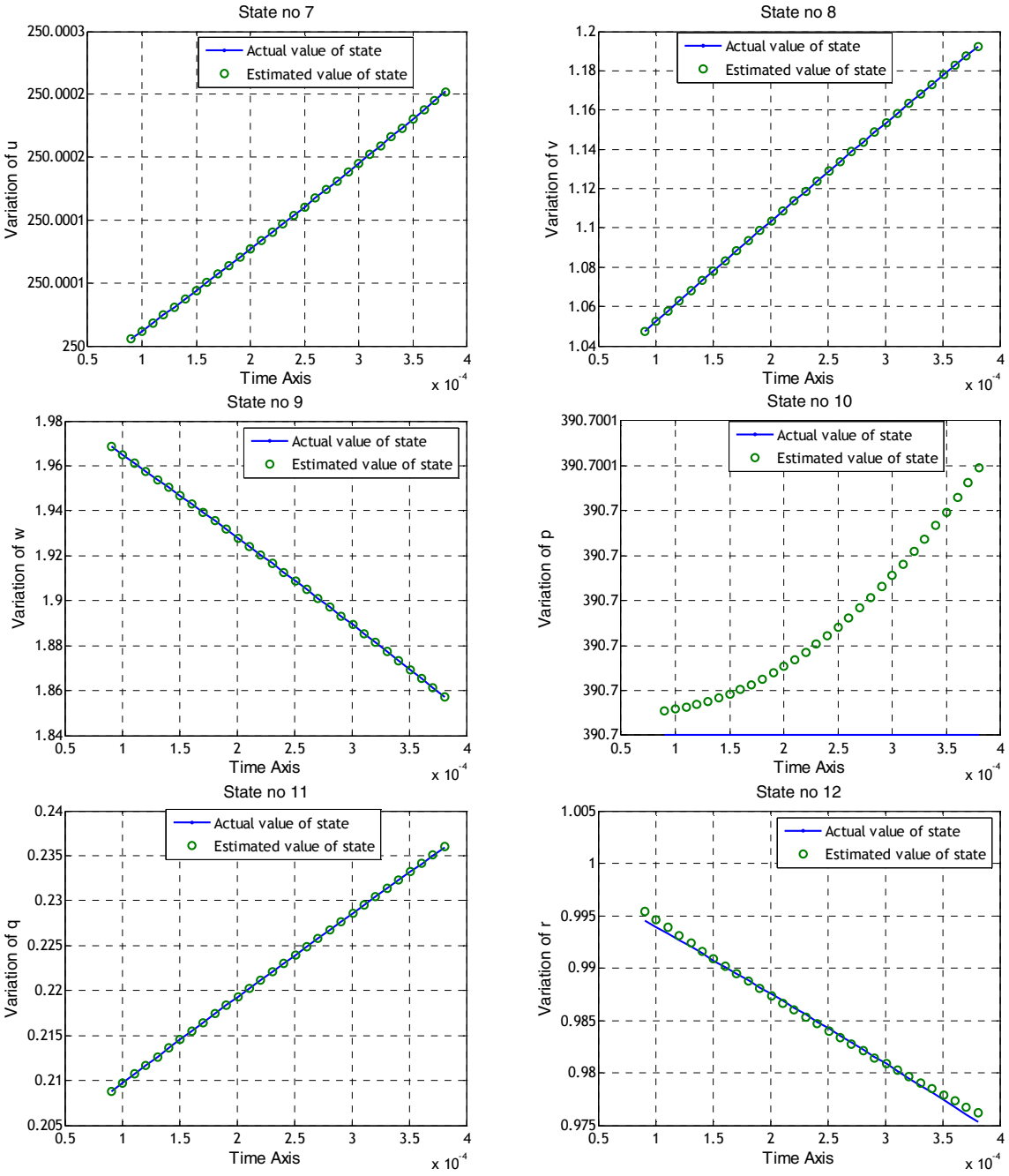

Figure 4.3: Estimates of last six states for Bar Magnet magnetic field

4.2.2. Rectangular Loop Magnetic Field

This section presents the results of state estimation when the projectile is traveling in a magnetic field generated by current flowing through a 5cm by 3cm rectangular loop conductor, coiled around the muzzle of the launching gun. The magnetic field readings are obtained over 25 time steps by a sensor array having five magnetometers placed randomly on the projectile. The average of the final error over the 25 time steps is again found to be $2.88\times10^{-4}\%$. The graphical results are as shown in figure 4.4.

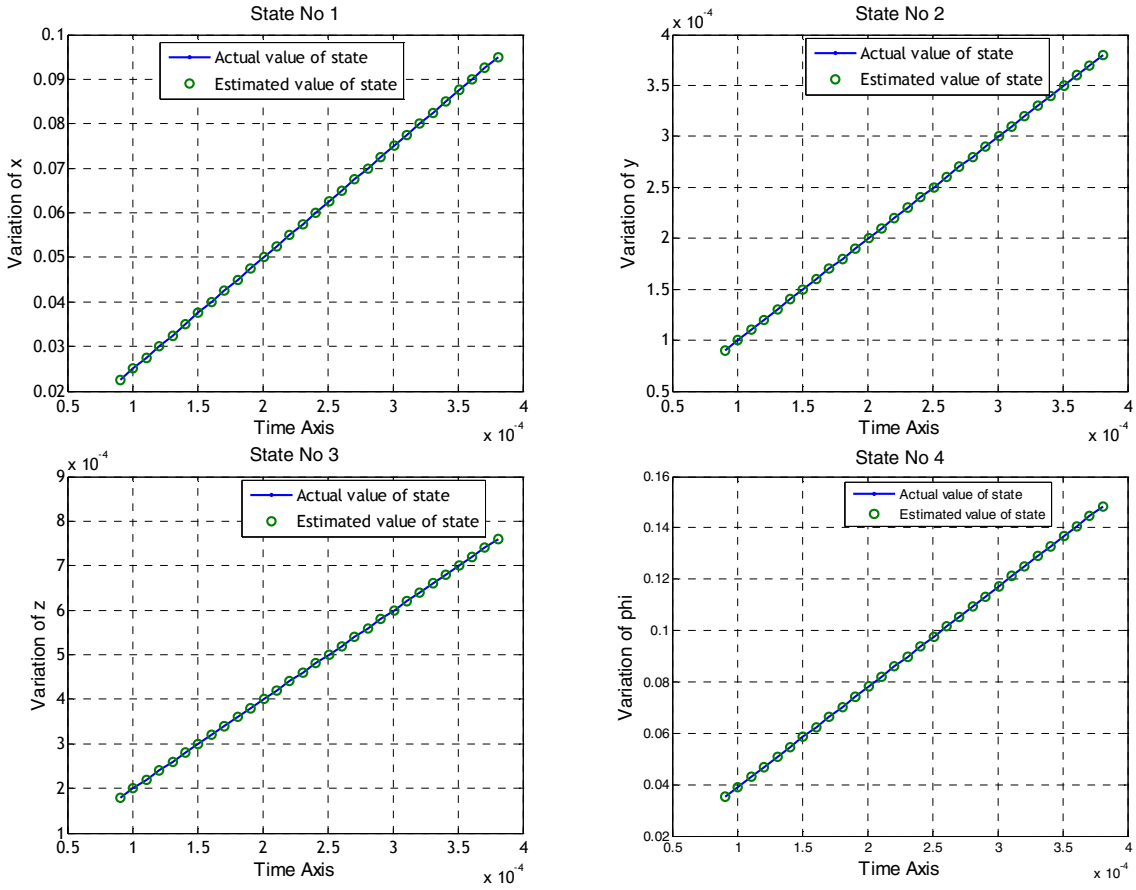

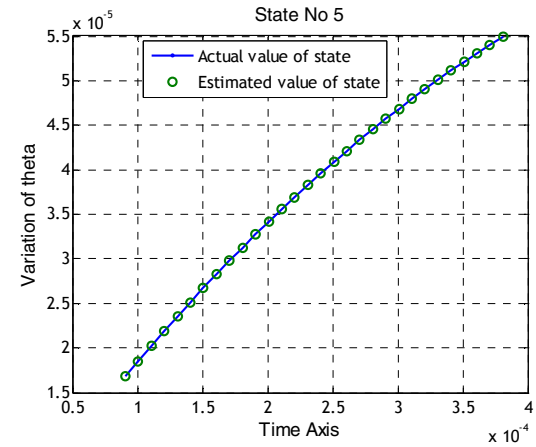
State No 5
x 10^-5
Actual value of state
Estimated value of state
Variation of theta
Time Axis
x 10^-4

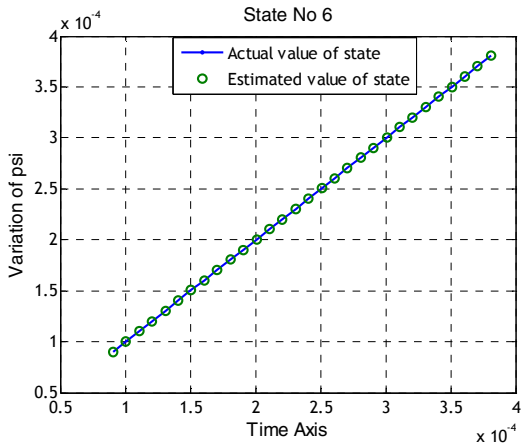
State No 6
x 10^-4
Actual value of state
Estimated value of state
Variation of psi
Time Axis
x 10^-4

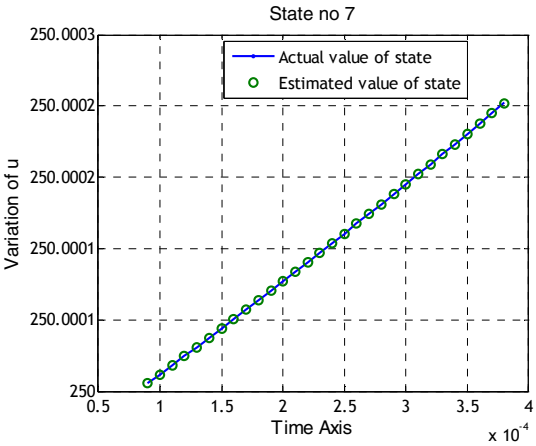
State no 7
Actual value of state
Estimated value of state
Variation of u
Time Axis
x 10^-4

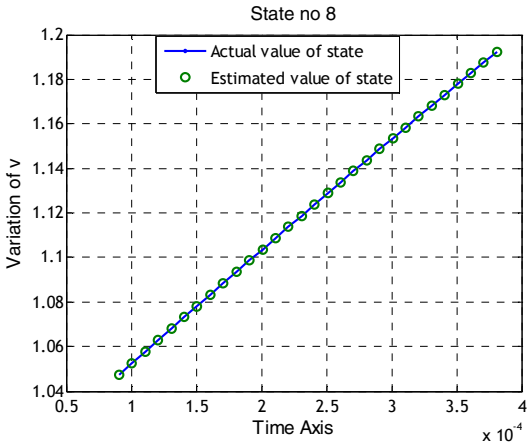
State no 8
Actual value of state
Estimated value of state
Variation of v
Time Axis
x 10^-4

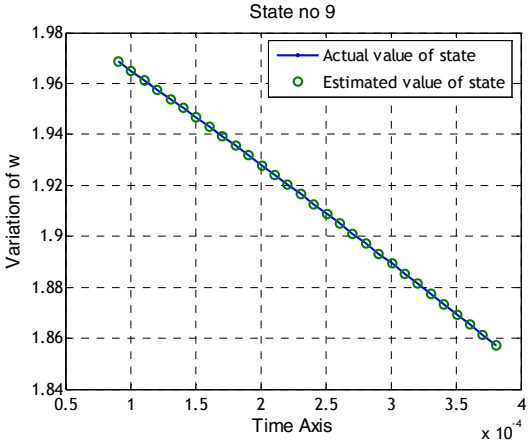
State no 9
Actual value of state
Estimated value of state
Variation of w
Time Axis
x 10^-4

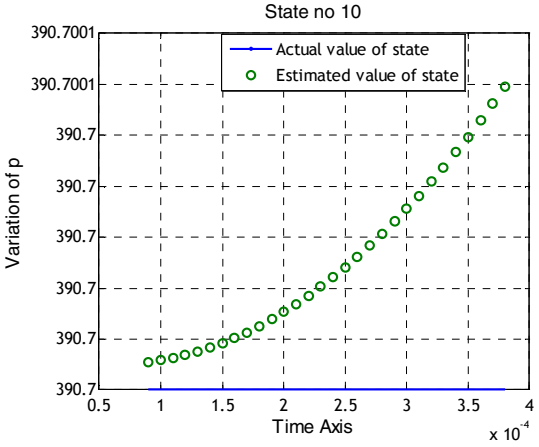
State no 10
Actual value of state
Estimated value of state
Variation of p
Time Axis
x 10^-4

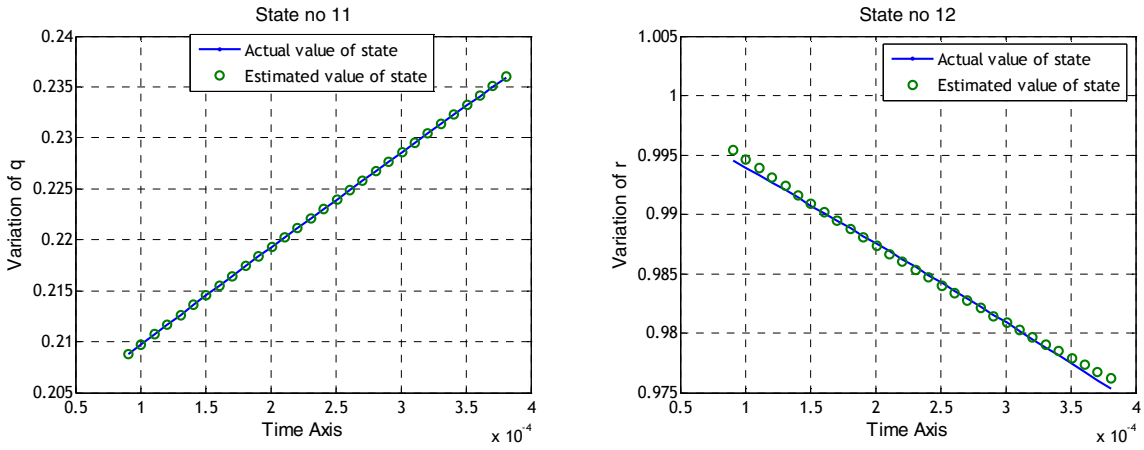

Figure 4.4: Estimates of the projectile states for Rectangular Loop magnetic field

Thus, both bar magnet and rectangular loop generated fields show exactly same results when sensor data is perfect.

4.3. State Estimation with Sensor Noise

When sensor noise is present estimation of projectile state is dependent upon the percentage of noise present in the sensor readings. This section presents the results of state estimation with rectangular loop and bar magnet generated magnetic fields when sensor noise is present.

4.3.1. Bar Magnet Magnetic Field

The estimation error is directly dependent on the amount of noise added to the sensor readings. This section presents the estimation results for a projectile traveling in a

magnetic field generated by a bar magnet placed on the top of the muzzle of the launching gun. The magnetic field readings are obtained over 25 time steps by a sensor array having five triaxial magnetometers placed in a ring around the projectile.

The sensor readings are corrupted by zero mean, white gaussean noise which is approximately $10^{-4}\%$ of the sensor readings. This is found to be the highest level of noise that this system could tolerate, within reasonable error bounds. The average of the final error over the 25 time steps is found to be 0.05%, which is considerably higher than the no noise case. The graphical results are as shown in figure 4.5.

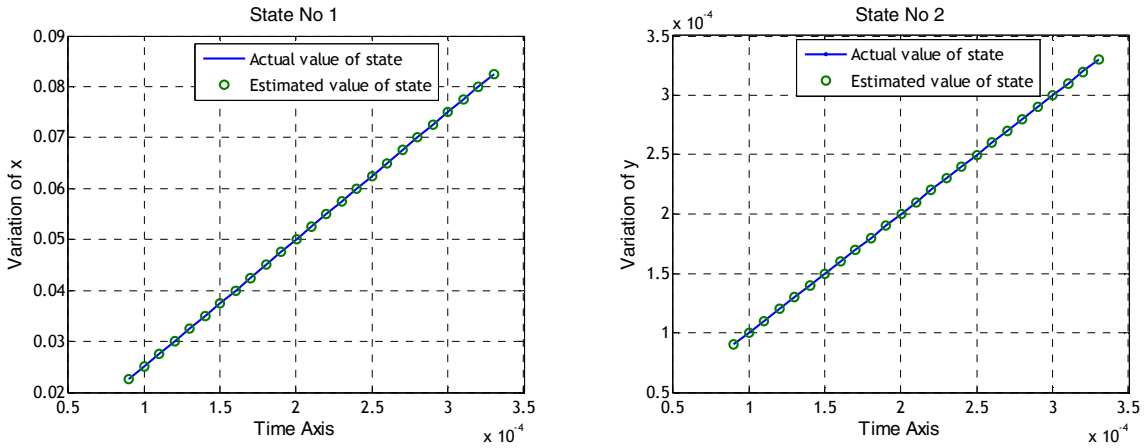

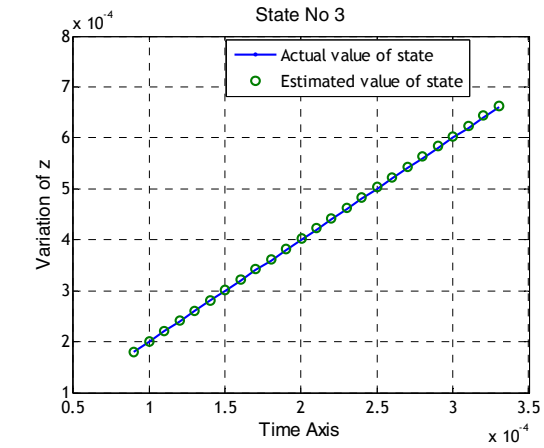
State No 3
x 10^-4
Actual value of state
Estimated value of state
Variation of z
Time Axis
x 10^-4

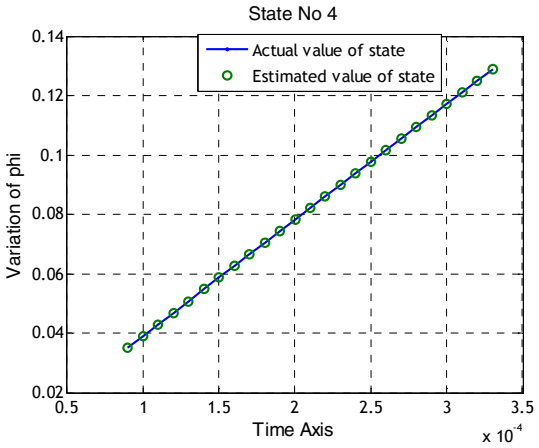
State No 4
Actual value of state
Estimated value of state
Variation of phi
Time Axis
x 10^-4

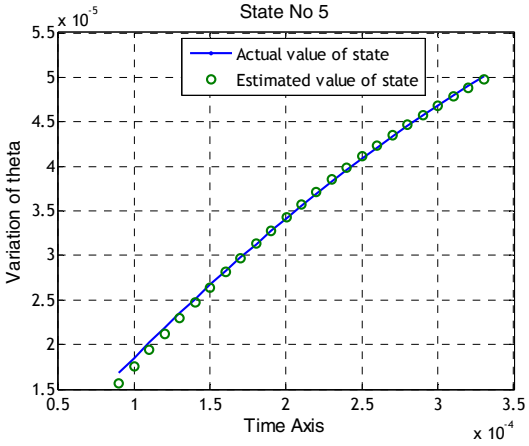
State No 5
x 10^-5
Actual value of state
Estimated value of state
Variation of theta
Time Axis
x 10^-4

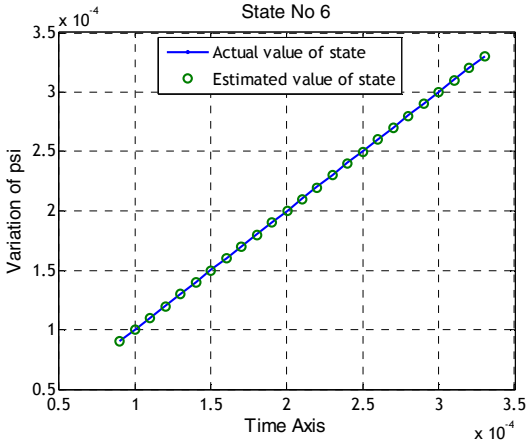
State No 6
x 10^-4
Actual value of state
Estimated value of state
Variation of psi
Time Axis
x 10^-4

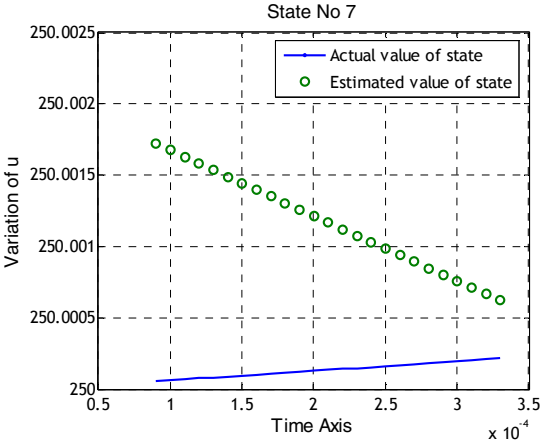
State No 7
Actual value of state
Estimated value of state
Variation of u
Time Axis
x 10^-4

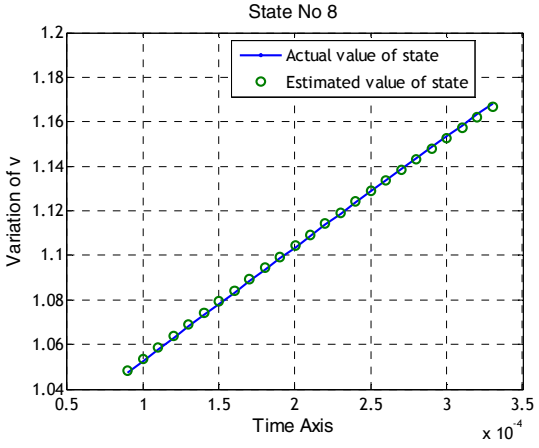
State No 8
Actual value of state
Estimated value of state
Variation of v
Time Axis
x 10^-4

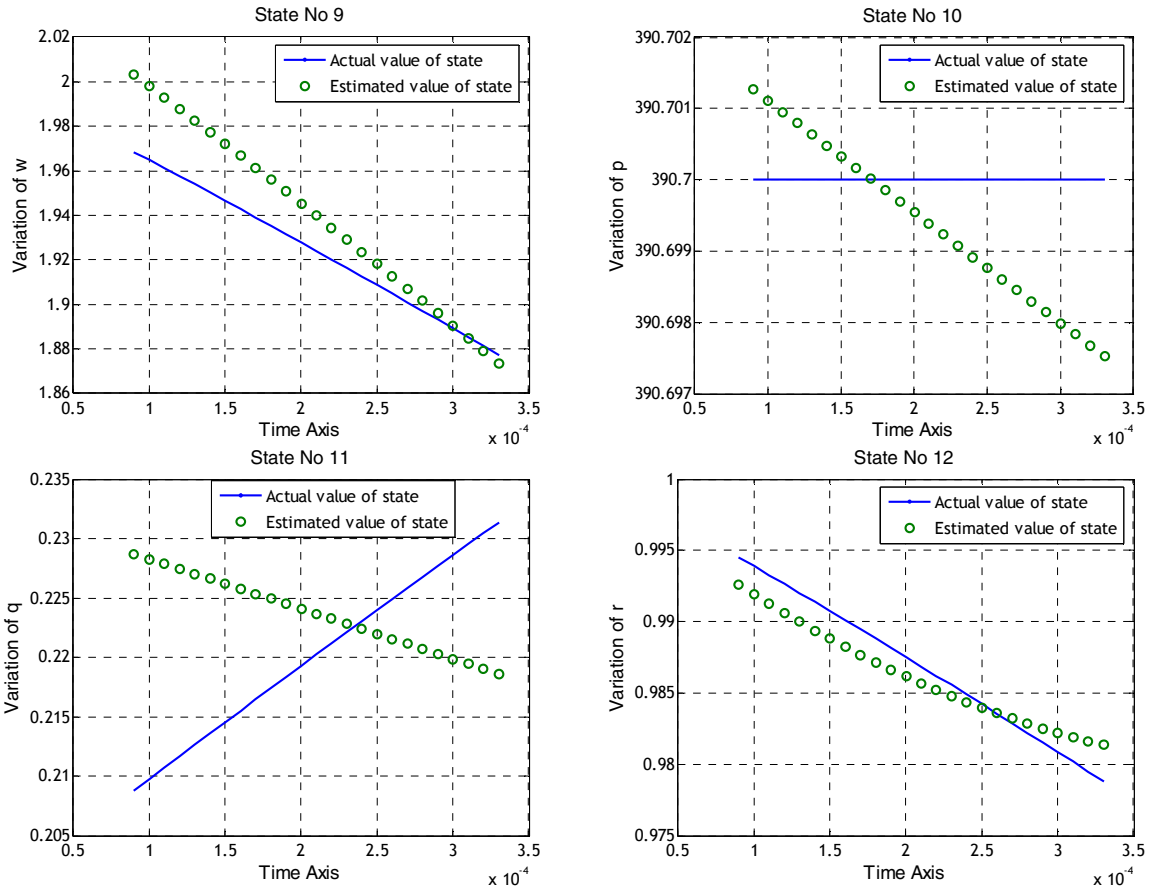

Figure 4.5: Estimates of Projectile States with 10^{-4}*% sensor noise with Bar Magnet magnetic field*

4.3.2. Rectangular Loop Magnetic Field

This section presents the estimation results for a projectile traveling in a magnetic field generated by current flowing through a 5cm by 3cm rectangular loop conductor, coiled around the muzzle of the launching gun. The magnetic field readings are obtained over 25 time steps by a sensor array having 11 rings, each having 36 magnetometers,

placed around the projectile, and 3 rings, each having 24 magnetometers, embedded inside the projectile.

The sensor readings are corrupted by zero mean, white gaussean noise which is approximately 0.1% of the sensor readings. This is found to be the highest level of noise that this geometry could tolerate, within reasonable error bounds. The average of the final error over the 30 time steps is approximately found to be 0.05% . Thus, the estimate results for a square loop generated magnetic field are considerably better than those for a bar magnet generated field in the case of noisy sensor readings. The graphical results are as shown in figure 4.5.

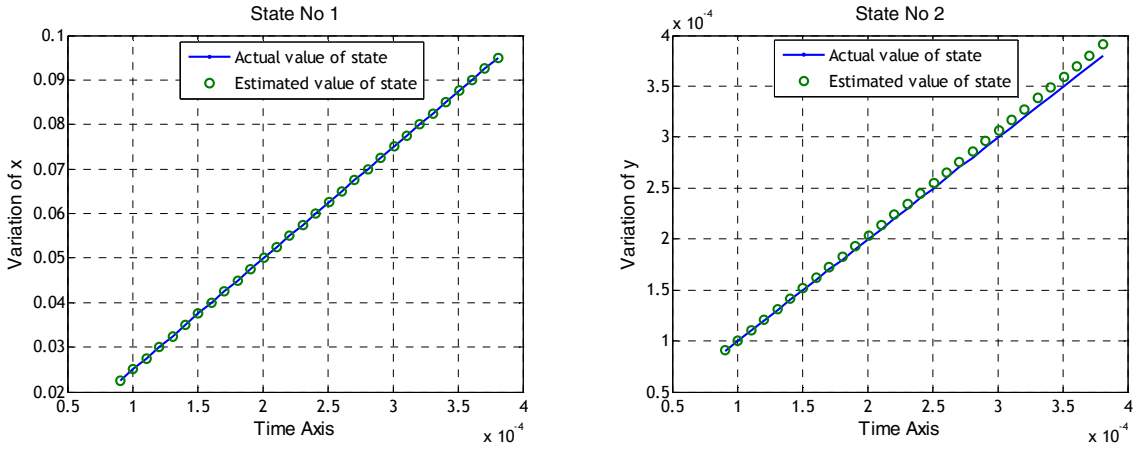

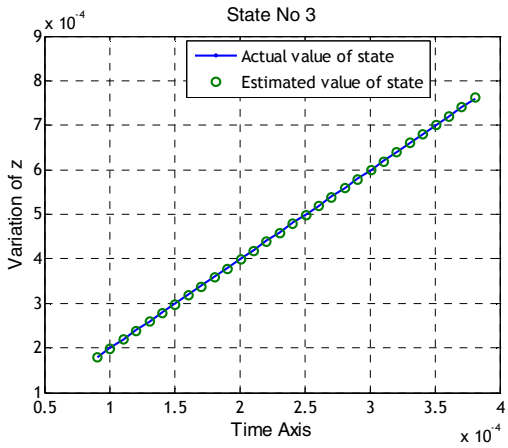
State No 3
Actual value of state
Estimated value of state
Variation of z
Time Axis
x 10^-4

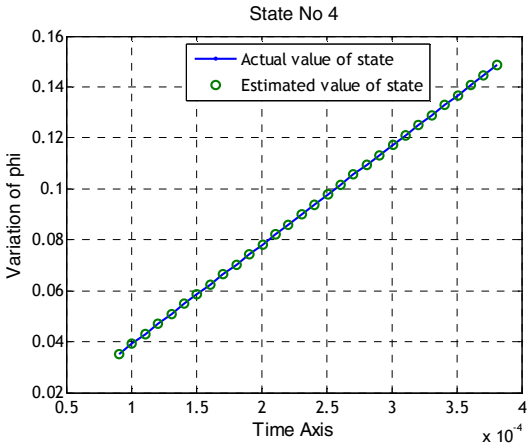
State No 4
Actual value of state
Estimated value of state
Variation of phi
Time Axis
x 10^-4

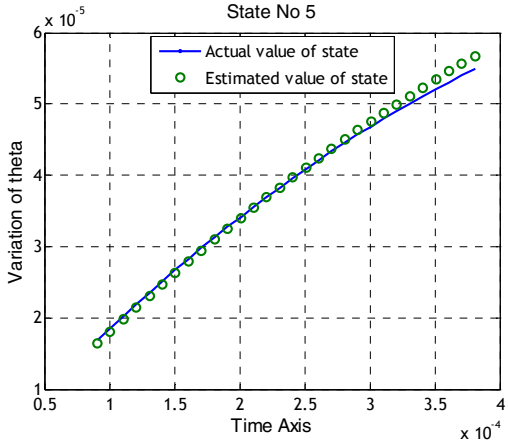
State No 5
Actual value of state
Estimated value of state
Variation of theta
Time Axis
x 10^-4

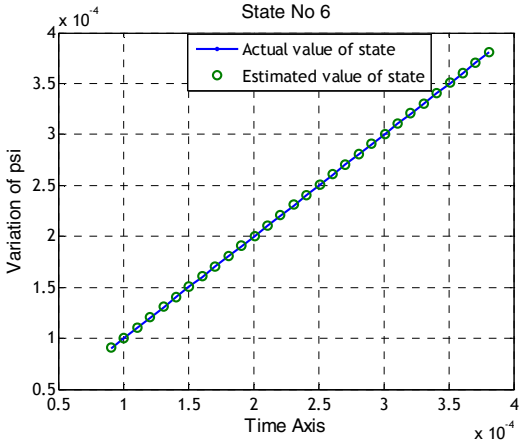
State No 6
Actual value of state
Estimated value of state
Variation of psi
Time Axis
x 10^-4

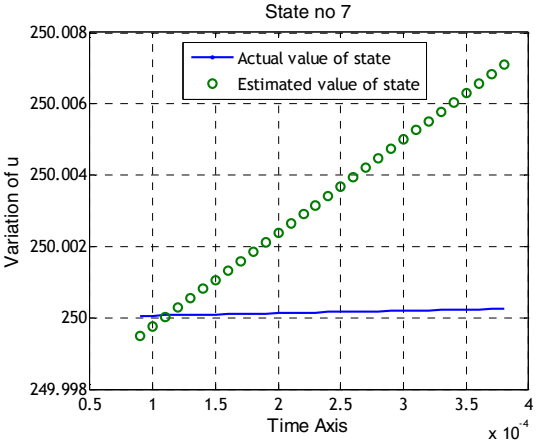
State no 7
Actual value of state
Estimated value of state
Variation of u
Time Axis
x 10^-4

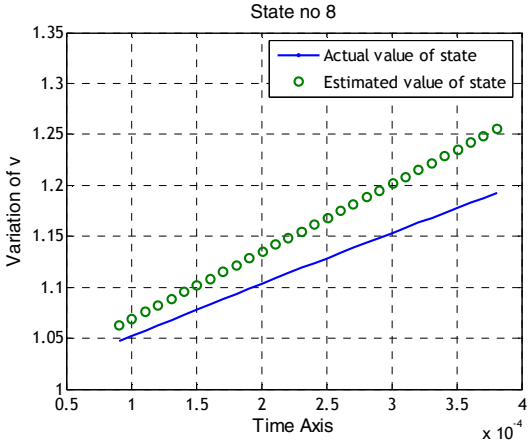
State no 8
Actual value of state
Estimated value of state
Variation of v
Time Axis
x 10^-4

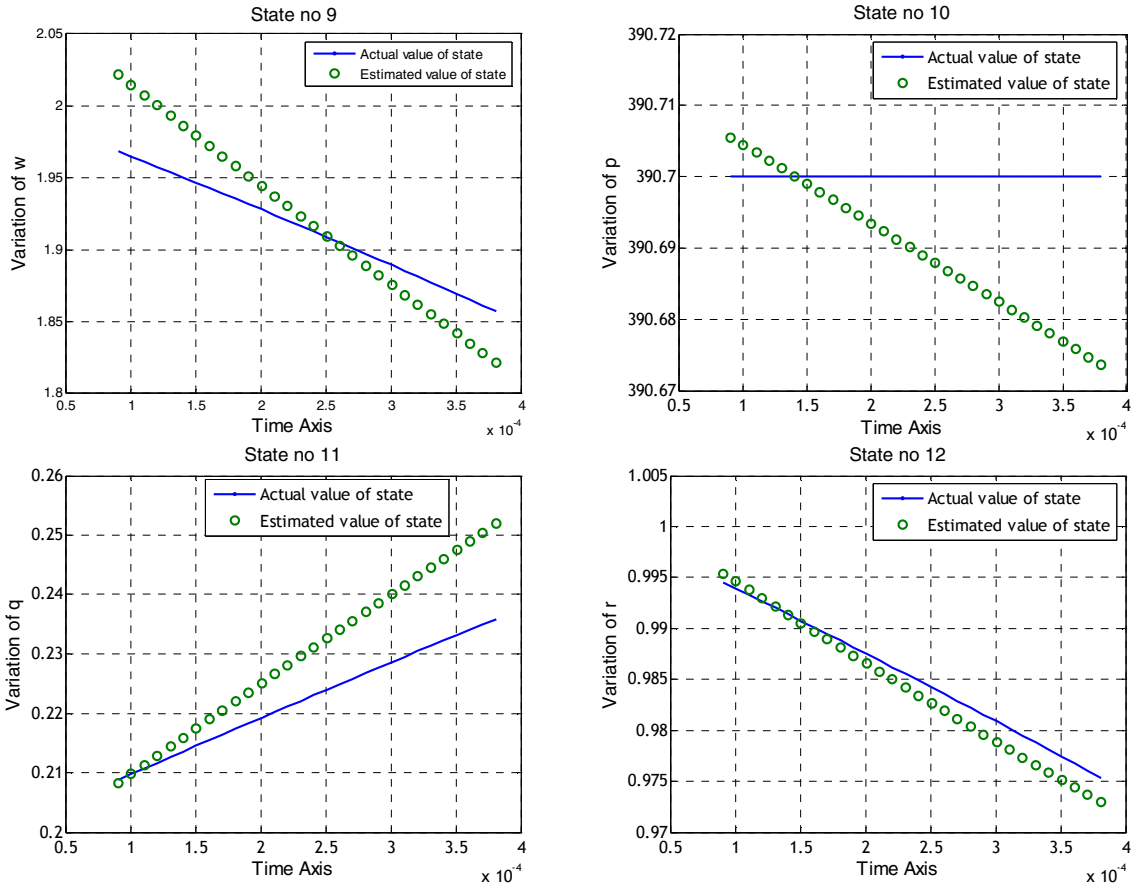

Figure 4.6 Estimates of Projectile States with 0.1% *sensor noise with Rectangular Loop magnetic field*

Since rectangular loop magnetic field generates better state estimates as compared to bar magnet magnetic field, we will use the rectangular loop magnetic field for all results henceforth, unless specified. The magnetic field readings will be obtained from a sensor array having 11 rings, each having 36 triaxial magnetometers, placed around the projectile, and 3 rings, each having 24 triaxial magnetometers, embedded inside the projectile.

4.4. Trade Studies

This section describes how the accuracy of the estimation varies according to changes in various factors such as, noise levels, period of data burst, and sensor geometry. Since the rectangular loop performs better in noisy conditions, the trade studies are performed using the *rectangular loop magnetic field*.

4.4.1. Variation of Error with Sensor Noise Level

The estimation accuracy decreases as sensor noise levels are increased. The final error of estimation increases linearly with sensor noise. This can be seen from Figure 4.7, which shows the average of the final error over 25 time instants for several noise levels. The final error plotted is also calculated as a percentage of the actual state readings. Noise is measured as a percentage of exact magnetometer sensor data.

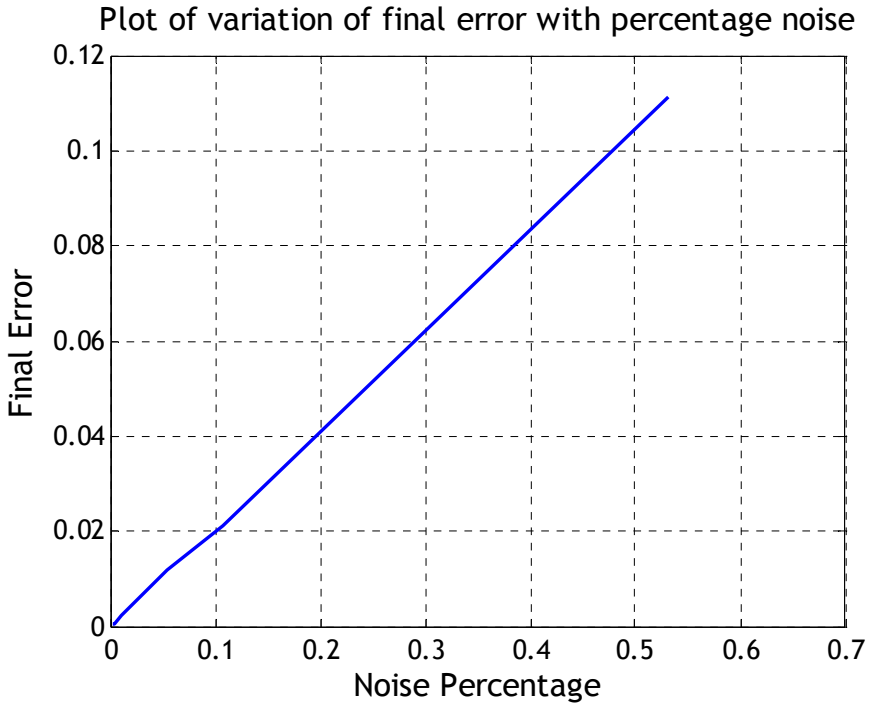

Figure 4.7: Variation of Error in Estimate with Sensor Noise

Since the error variation at low noise levels is not very clear from the figure, Figure 4.8 has been included to show the steady increase of the error with noise percentage at extremely low noise levels.

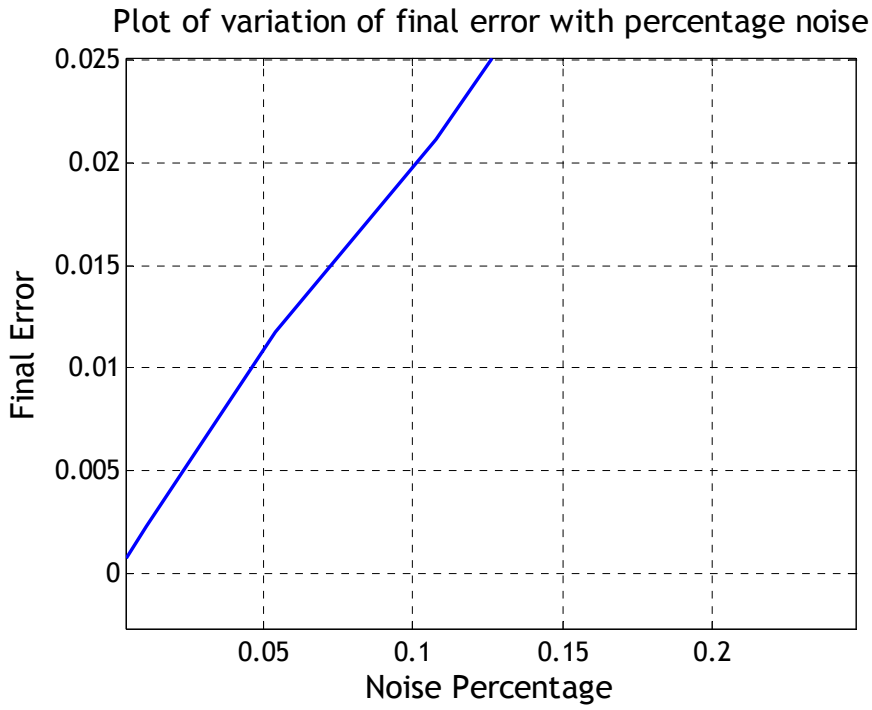

Figure 4.8: Variation of Error in Estimation of State Vales at Low Noise Levels

4.4.2. Variation of Error with Data Burst Period

Data burst period plays a very important role in determining the accuracy of the state estimate. The period of data burst required is dependent upon the sensor noise levels. In low noise conditions, a lower data burst period gives a more accurate result than a high period, since increasing the number of time steps also increases the nonlinearities in the sensor readings and state values. However, at high noise levels, a longer period of data burst works better since estimation of the last six states by using nonlinear regression (described in section 3.5.2) is more accurate with higher number of data points. Fitting a curve through the first six states also acts as a crude form of filtering

out the noise, and this filtering effect overshadows the ill-effects of nonlinearities to a certain extent.

This can be seen more clearly from a comparison of figures 4.9 and 4.10. Figure 4.9 shows the variation of final error with respect to data burst period in the case of magnetometer readings corrupted by 0.03% noise. Figure 4.10 shows the same results for sensor readings without any noise. It can be seen from the two figures that while the error falls in the first case, it increases steadily in the second.

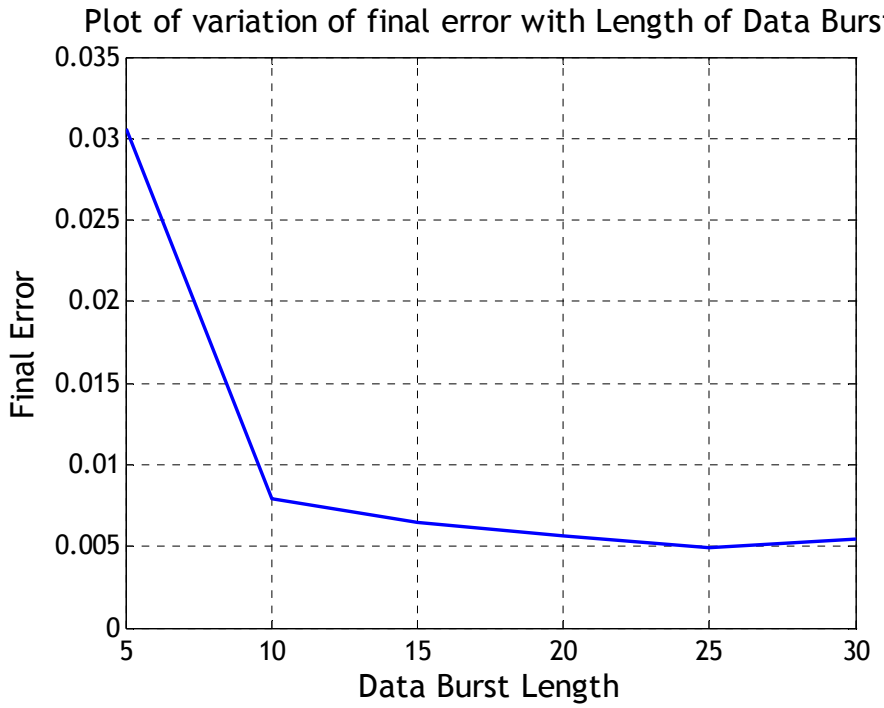

Figure 4.9: Variation of Final Error with Data Burst Length with magnetometer readings corrupted by 0.03% Noise

It can be seen from Figure 4.9 that as the number of data points is increased, the final error in estimation decreases. This fall in the error is almost quadratic. However, after data burst length of 25, the error begins to increase again. This is because after this point the positive effects of the crude filtering described earlier can no longer overshadow the effects of increasing nonlinearities in the data.

Figure 4.10: Variation of Final Error with Data Burst Length with accurate magnetometer sensor readings

The results in Figure 4.10 are in a total contrast to those in Figure 4.9. When there is no sensor noise, the final error increases steadily with the number of data points, because there is no effect of filtering, since no sensor noise is present.

4.4.3. Variation of Error with Number of Magnetometers

The number of magnetometers and the arrangement of sensors on the projectile also have an effect on the accuracy of the state estimate when sensor data is noisy. This is because certain geometries generate a better signal to noise ratio compared to others. In general, increasing the number of magnetometers in the sensor array leads to an increase in accuracy of the method. This can be seen more clearly from Figure 4.11, which shows the results for the state estimation with approximately 0.03% sensor noise.

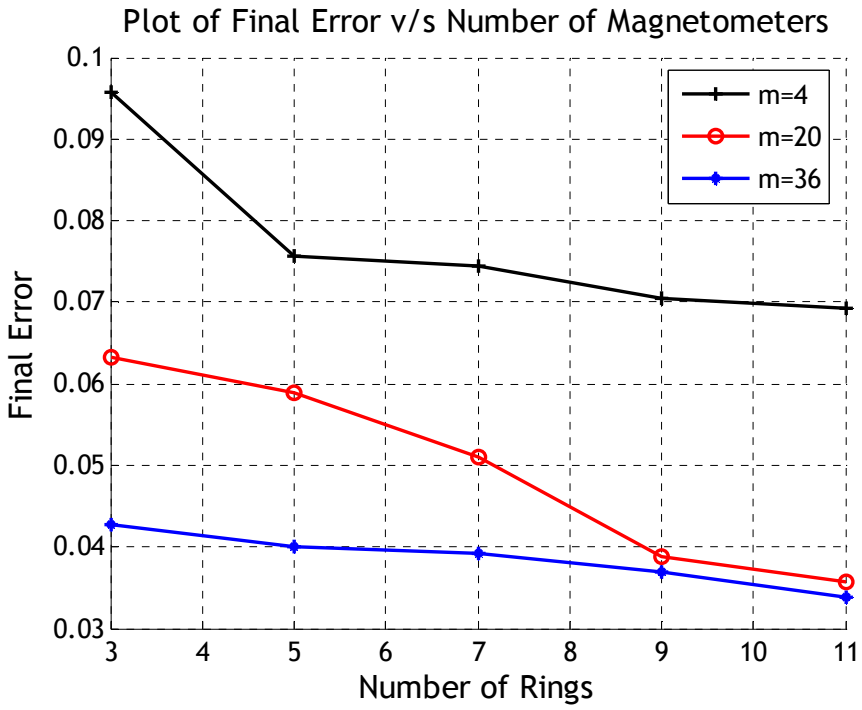

Figure 4.11: Variation of Final Error with Number of Magnetometer Sensors

Figure 4.11 presents the results for sensor geometry with 'n' rings, each having 'm' triaxial magnetometers fixed symmetrically on the projectile. The results show that as the number of rings (n) is increased, the error decreases. Also, increasing the number of magnetometers per ring (m) causes the error to decrease steadily.

5. CONCLUSION

This chapter discusses the results presented in Chapter 4 and the utility of the magnetometer sensor system for estimating initial state of gun launched projectiles. It also presents the further improvements that can be made to the design and scope for future work related to this system.

5.1. Discussion of the Results

The results shown in Chapter 4 indicate that the suggested solution to the initial state estimation problem works very well for a no noise case, irrespective of the sensor geometry, number of magnetometers and the magnetic field used. However, the results show a clear dependence on these design parameters when sensor noise in increased.

As the noise percentage of sensor readings is increased, the behavior of the system changes with the magnetic field used for the estimation. While a bar magnet generated magnetic field system can not withstand sensor noise higher than 0.0001%, the maximum sensor noise that the system can withstand with a rectangular loop generated field is approximately 0.1%. The rectangular loop magnetic field, thus, gives us practically usable results, since magnetometer sensors are known to be very accurate and noise levels are not expected to exceed this value.

The difference in the results for the two kinds of magnetic fields can be attributed to the spatial variation the fields. Figures 5.1-5.3 and 5.4-5.6 show the spatial variation of the bar magnet and square loop generated fields. It can be seen from the figures that the spatial variation of the square loop field is much more than the spatial variation of the bar magnet field. Thus, it can be concluded that the spatial variation of the magnetic field in which the projectile travels plays a very important role in the accuracy of the estimate.

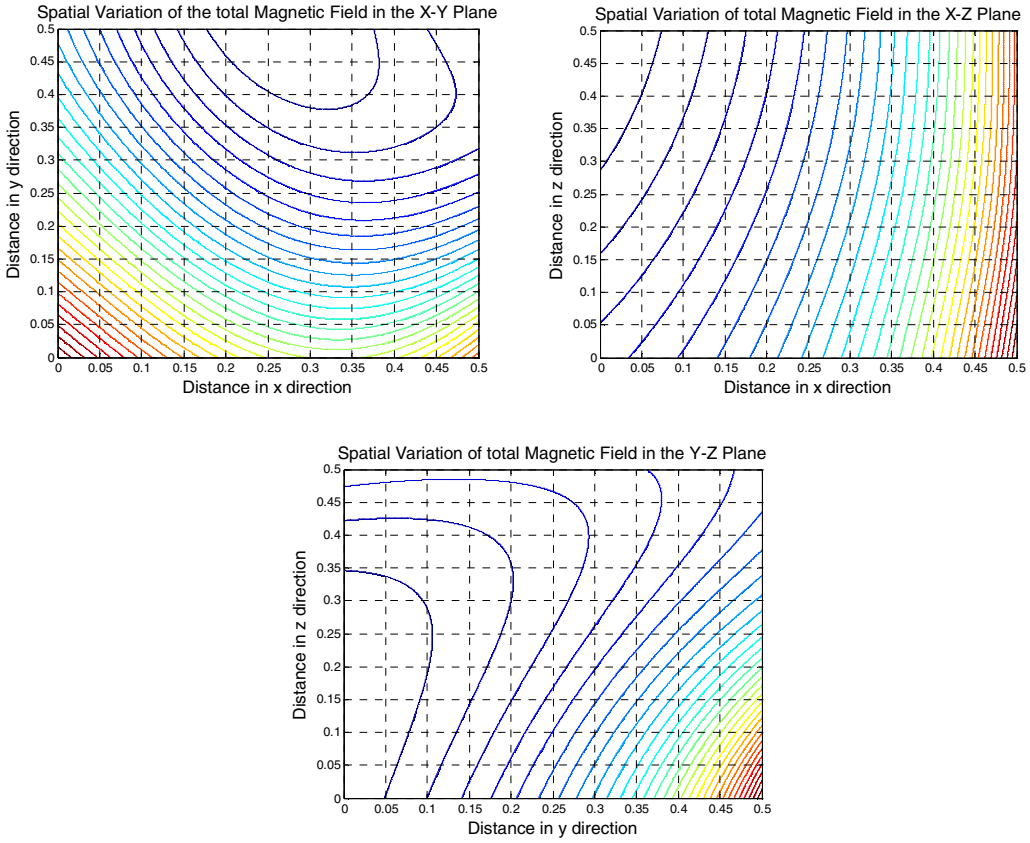

Figure 5.1: Plot of Magnetic Field generated by a Bar Magnet

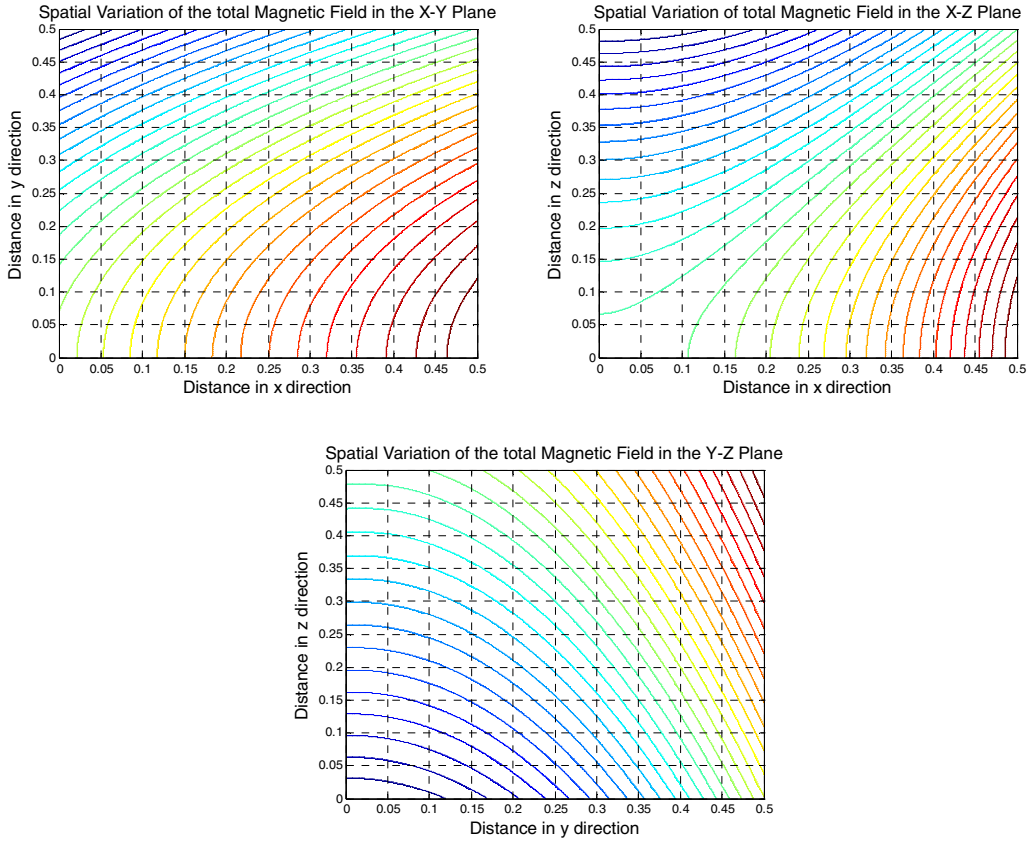

Figure 5.2: Plot of Magnetic Field generated by a Rectangular Loop

The number of magnetometers used, and the sensor geometry also have an effect on the estimation as sensor noise increases. This is because specific arrangements of the sensors on the projectile body help in canceling out the effects of sensor noise, and increasing the Signal to Noise Ratio (SNR). However, the magnetometer geometry that ensures good results at 0.1% sensor noise for a rectangular loop magnetic field does not seem to be practically realizable. This is because the number of magnetometers (468) is too high for a practical realization.

Moreover, apart from the sensor noise levels, the results of the estimation are highly dependent upon the data burst period and the number of sensors also. It is interesting to see how noise level affects the period of data burst required for an accurate estimate. In high noise cases, most of the error in estimation comes from the error in the last six states, and this can be overcome by using a larger data burst period. However, as can be seen from the results shown in Figure 4.9, errors due to nonlinearities start to set in if the data burst period is increased beyond a certain length.

5.2. Scope for Future Work

Most of the error in the state estimation process comes from the use of nonlinear regression in estimating the last six states from the first six states. Thus, the estimation accuracy can be improved by using more accurate signal processing algorithms for finding the derivative of the estimates of the first six states.

The effects of magnetic field properties on the estimate can be further investigated and magnetic fields that generate more accurate estimates can be found. Also, by studying the effects of sensor arrangements on signal to noise ratio, practically realizable sensor geometries, with fewer magnetometers, that give better state estimates could be found.

More methods to estimate subsets of the state vector could also be investigated. For example, a subset of the sensor suite could be switched on and off, estimating a part of the state vector each time, and finally the results could be combined to obtain a quicker and more accurate estimate of the complete state. A magnetometer sensor array could also be combined with other types of sensors such as accelerometers and gyroscopes to investigate the improvements in speed and accuracy of estimation.

BIBLIOGRAPHY

1. A. Balogh, C.M. Carr, M. H. Acuna, M. W. Dunlop, T. J. Beek, P. Brown, K. H. Fornacon, E. Georgescu, K. H. Glassmeier, J. Harris, G. Musmann, T. Oddy and K. Schwingenschuh, *"The Cluster Magnetic Field Investigation : In-Flight Performance and Initial Results"*, European Geophysical Society, 2001.

2. Neil M. Barbour, John M. Elwell and Roy H. Setterlund, *"Inertial Instruments – Where to Now?"*, In AIAA Guidance, Navigation and Control Conference, 1992, p. 566-574.

3. M. J. Caruso, *"Application of Magnetoresistive Sensors in Navigation Systems"*, Sensors and Actuators 1997, SAE SP-1220 (15-21), February 1997.

4. Mark Costello and Thanat Jitpraphai, *"Determining Angular Velocity and Angular Acceleration of Projectiles Using Triaxial Acceleration Measurements"*, Journal of Spacecrafts and Rockets, Vol. 39, No. 1 (73-89), 2002.

5. Jerry H. Ginsberg, *"Advanced Engineering Dynamics"*, Cambridge University Press, Second Edition.

6. Richard P. Hallion, "*Precision Guided Munitions and the New Era of Warfare*", Air Power Studies Center Working Papers.

7. William H. Hayt, Jr., *"Engineering Electromagnetics"*, Tata McGraw-Hill Publishing Company Limited, New Delhi, Fifth Edition.

8. Gary L. Katulka, *"Micro-electromechanical Systems and Test Results of SiC MEMS for High-g Launch Applications"*, Sensors, 2002, Proceedings of IEEE.

9. Thomas Kuhn, *"Aspects of Pure and Satellite Aided Inertial Navigation for Gun Launched Munitions"*, Position Location and Navigation Symposium, IEEE, 2004.

10. Roy R. Minor and David W. Rowe, *"Utilization of GPS/MEMS-IMU for Measurement of Dynamics for Range Testing of Missiles and Rockets"*, Position, Location and Navigation Symposium, IEEE 1998.

11. William H. Press, Saul A. Teukolsky, William T. Vetterling and Brian P. Flannery, *"Numerical Recipes in C – The Art of Scientific Computing",* Cambridge University Press, Second Edition.

12. Lloyd N. Trefethen, David Bau III, *"Numerical Linear Algebra"*, Society for Industrial and Applied Mathematics.